From recovered palladium to molecular and nanoscale catalysts

Khairil A. Jantan,[a,b+] Kuang Wen Chan,[a+] Laura Melis,[c] Andrew J. P. White,[a] Luciano Marchiò,[d] Paola Deplano,[e] Angela Serpe[c]* and James D. E. T. Wilton-Ely[a]*

[a] *Department of Chemistry, Imperial College, Molecular Sciences Research Hub, White City Campus, London W12 0BZ, UK. E-mail: j.wilton-ely@imperial.ac.uk*
[b] *Faculty of Applied Sciences, Universiti Teknologi MARA (UiTM), 40450 Shah Alam, Malaysia.*
[c] *Dipartimento di Ingegneria Civile, Ambientale ed Architettura, INSTM, University of Cagliari, Via Marengo 2, I09123, Cagliari, Italy E-mail: serpe@unica.it*
[d] *Dipartimento di SCVSA, University of Parma, Parco Area delle Scienze 17A, I43124 Parma, Italy.*
[e] *Dipartimento di Fisica, University of Cagliari, SS 554 Bivio per Sestu, I-09042, Monserrato, Cagliari, Italy.*

+ Equal contribution

Abstract

[PdI_2(Me_2dazdt)] is obtained from palladium powder via a 100% atom economical Pd(0) leaching reaction using Me_2dazdt (*N,N'*-dimethyl-perhydrodiazepine-2,3-dithione) and iodine. This complex is a versatile starting point for ligand exchange reactions with (di)phosphines, yielding *trans*-[$PdI_2(PPh_3)_2$] and [PdI_2(dppe)] (dppe = 1,2-bis(diphenylphosphino)ethane). Further reaction with dithiocarbamates provides compounds of the form [Pd(DTC)$(L)_n$]+ (DTC = dithiocarbamate; L = PPh_3, n = 2; L = dppe, n = 1), which are highly active catalysts for regio- and chemo-selective C-H bond activation reactions. Using DTC ligands with trimethoxysilyl-terminated tethers, the palladium(II) units can be attached to the surface of core-shell, silica-coated Fe_3O_4 nanoparticles. Once tethered, these units formed the catalytically-active component of a recyclable, quasi-heterogeneous, Pd(II)-based catalytic system based on recovered palladium, illustrating the proposed circular model strategy. These investigations contribute to key steps in this process, such as efficient, atom-economical recovery, chemoselectivity of ligand substitution reactions, demonstration of catalytic activity and the potential for immobilization of catalytic surface units derived from recovered metal.

Keywords

Metal recovery, catalysis, palladium, dithiocarbamates, immobilization

Introduction

Regulation to encourage the adoption of improved and safer processes to reduce or eliminate pollution and safeguard the availability of elements is spreading worldwide.[1] This stipulates that industrial processes should embrace the use of sustainable and efficient reactions which produce low levels of waste and promote the recycling of materials. Catalytic transformations in organic synthesis provide a key example of how lowering the activation barrier of a reaction can reduce the amount of energy required.[2] At the same time, one of the most widely-held concerns in organic synthesis is the use of costly and rare metals for catalysis.[3] These metals play a critical role in many important industrial processes. For example, palladium plays a central role in the catalysis of cross-coupling reactions[4-6] and thus contributes greatly to the industrial production of pharmaceuticals. Nevertheless, palladium is a high cost 'critical' element due to its limited and geographically-localized availability, coupled with its world-wide economic importance. Its most widespread application is in the catalytic converters (Three Way Catalysts, TWCs) used to limit the environmental impact of automotive emissions.[3] This use represents 85% of the total demand from palladium-based applications and the demand for palladium for TWCs alone exceeds the global annual supply of the metal from existing mines.[7] A further relevant and growing application is in electric and electronic equipment (EEE), which accounts for 10% of the demand for palladium.[7] In this setting, palladium is used as a plating material for connectors in conductive tracks in hybrid integrated circuits (HIC), often paired with silver. In multi-layer ceramic capacitors (MLCC), it represents the most effective and durable material for conductive electrode layers. Alongside this is the long-standing use of palladium for chemicals and dentistry. This large consumption of the metal has driven attempts to find suitable non-noble metal catalysts, such as in homogeneous or heterogeneous catalytic processes.[3] As an alternative, increasing attention has been devoted recently to the synthesis of more easily recoverable quasi-heterogeneous catalysts.[8] In particular, catalytic units immobilized on the surface of magnetic nanoparticles (MNP) have been shown to be active catalysts for a variety of chemical reactions, with recovery being effected by the application of a handheld magnet.[9] This type of catalysis combines both the advantages of homogeneous and heterogeneous catalysis. By keeping the size of the support in the nanoscale range, it exposes a high effective surface area, allow reaction to occur in a 'homogeneous' manner. At the same time it provides a straightforward means of recovery as is typical for heterogeneous catalysts.[8]

In this contribution, we present the results of the synthesis, characterization and catalytic activity of new immobilized Pd(II) catalysts, based on *S,S*-chelating

dithiocarbamate (DTC) donor ligands on the surface of silica-coated Fe_3O_4 nanoparticles. The use of sulfur-containing ligands in catalysis remains uncommon, possibly due to fears over catalyst poisoning, prevalent mainly in heterogeneous catalysis. Nonetheless, literature reports have demonstrated that Pd(II) complexes with bidentate sulfur ligands can catalyze reactions such as C-H activation. This is exemplified by the use of palladium imidazol(in)ium-2-dithiocarboxylate complexes to catalyze the C-H oxidative functionalization of benzo[*h*]quinoline to 10-methoxybenzo[*h*]quinoline.[10] These complexes were found to be as effective as the [$Pd(OAc)_2$] typically employed in such reactions.[11,12] These investigations have been extended to catalysts supported by dithiocarbamate ligands,[13] which are simple and straightforward to prepare.[14-16] Moreover, in tune with the 'circular economy' concept, which aims to limit the use of critical raw materials,[17] we will show how it is possible to use a Pd recovery product, derived from a different kind of secondary resources (such as spent automotive three-way catalysts, WEEE etc.) as precursors for the catalytic moiety. This approach makes the palladium recycling process itself more sustainable. Indeed it has been shown that palladium can be successfully leached using mixtures of halogens and sulfur-donating chelating ligands, particularly by cyclic and acyclic dithioxamides, in common organic solvents.[18] Among them, the most effective system for palladium leaching was found to be the Me_2dazdt·$2I_2$ adduct (Me_2dazdt = *N,N'*-dimethyl-perhydrodiazepine-2,3-dithione), which is able to dissolve almost quantitatively palladium metal powder at room temperature (10 mg, r.t., acetone, 1:2 Pd/adduct molar ratio) in less than two hours. The same amount of palladium can be dissolved in milled, spent TWC material by refluxing in methyl ethyl ketone (MEK) for 168h, in both cases leading to the complex [$Pd(Me_2dazdt)_2$](I_3)$_2$.[19] These leaching reactions are highly selective for palladium and are very promising for practical applications due to the low environmental impact of the reactants and working conditions,[20] in contrast to the dangerous and energy-intensive conventional pyro- and hydrometallurgical methods used in industry.[21-23] The palladium complexes obtained from these sustainable leaching reactions have recently been demonstrated to work very well in homogeneous Pd(II)-catalyzed C-H activation[13] and as suitable precursors of Pd(0) photocatalysts for H_2 production.[24] These discoveries were the starting point for this contribution, which explores the potential of using the recovery products as precursors for a new magnetically-recoverable catalyst system. In light of this aim in particular, we found that a promising new palladium recovery product, the heteroleptic compound, [PdI_2(Me_2dazdt)], could be conveniently obtained in high yield by treating metallic palladium with Me_2dazdt and I_2 in a 1:1:1 molar ratio. This valuable recovered compound proved to be a suitable precursor for the immobilized catalytic moieties and

represents the recovery product of choice for this work. It was decided to use the regio- and chemo-selective methoxy functionalization of benzo[*h*]quinoline (Scheme 1) as the benchmark reaction to compare the catalytic performance of homogeneous (non-immobilized) complexes and heterogenized (immobilized) molecular species.

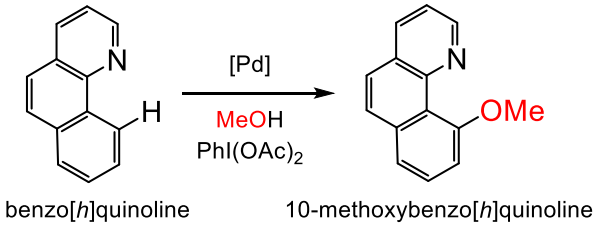

Scheme 1. Functionalization of benzo[*h*]quinoline in methanol with a Pd(II) catalyst and $PhI(OAc)_2$ as the oxidant.[11]

Dithiocarbamate-based Pd(II) catalysts were selected as promising for this purpose, due to their demonstrated catalytic activity in this reaction,[13] as well as the versatility offered by these ligands with regard to the incorporation of additional functionality (e.g., tethering groups) at the NR_2 unit.[14]

Results and discussion

Trimethoxysilyl-functionalized dithiocarbamate ligands K[**L1**] and K[**L2**] were prepared by treating the parent amines, *N*-methylaminopropyltrimethoxysilane and bis[3-(trimethoxysilyl)propyl]amine with carbon disulfide (Scheme 2). The ligands were fully characterized by ^1H and $^{13}C\{^1H\}$ NMR and IR spectroscopy, mass spectrometry and elemental analysis (Supporting Information).

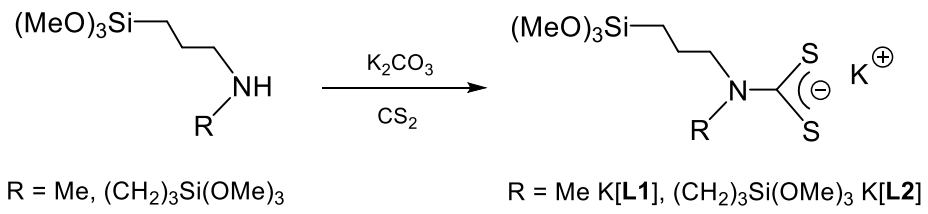

Scheme 2: Reaction between *N*-methylaminopropyltrimethoxysilane and bis[3-(trimethoxysilyl)propyl]amine and CS_2 under ambient conditions to form K[**L1**] and K[**L2**], respectively.

For this reaction ^1H NMR analysis proved particularly diagnostic with a clear downfield shift of the proton peaks, compared to the same features in the precursors, and disappearance of the amine protons at around 3.3 ppm. Moreover the resonances

due to the protons adjacent to the nitrogen atoms are shifted downfield to a larger extent than the peaks for the other protons of the chain (2.5 ppm to 4 ppm), indicating the formation of the new N-CS_2 bond. The solid state infrared spectrum also provided evidence for the successful formation of the dithiocarbamate salts with characteristic absorptions observed for the *v*(C-N), *v*(NC=S) and *v*(C-S) vibrational modes at 1460, 1250 and 960 cm^{-1}, respectively.[14,25] The overall formulation for **1** and **2** was confirmed by CHN elemental analysis and mass spectrometry, which showed molecular ions at m/z 268 and m/z 416, respectively.

Synthesis of palladium(II) complexes. Scheme 3 summarizes the strategy for the synthesis of the complexes to be employed in catalysis, starting from both a commercial salt, *cis*-[$PdCl_2(PPh_3)_2$], and a palladium recovery complex, [$PdI_2(Me_2dazdt)$] (**5**). Complexes **3** and **4** were prepared accordingly to Scheme 3, which shows the addition of K[**L1**] and K[**L2**] to *cis*-[$PdCl_2(PPh_3)_2$] in the presence of NH_4PF_6. Complexes **3** and **4** were fully characterized by ^{1}H NMR, $^{13}C\{^1H\}$ and $^{31}P\{^1H\}$ NMR and IR spectroscopy as well as mass spectrometry and elemental analysis. The ^{1}H and $^{31}P\{^1H\}$ NMR spectra both showed an upfield shift in their resonances due to the electron back-donation from the palladium center to the dithiocarbamate ligand[26] and the σ-donation of the adjacent dithiocarbamate ligand. In addition to the new resonance observed at 30.5 ppm for both **3** and **4** in the $^{31}P\{^1H\}$ NMR spectra, the presence of the hexafluorophosphate counteranion was evidenced by a characteristic septet. $^{13}C\{^1H\}$ NMR analysis revealed characteristic low-field singlets for the CS_2 carbon nuclei at around 203 ppm. Further support for the formulation came from the solid state infrared spectra, which showed the presence of typical vibrational modes for phenyl rings attached to the phosphorous center (1000 and 1470 cm^{-1}) and the *v*(P-F) vibrational mode of the PF_6^- counter-ion (830 cm^{-1}).[27,28]

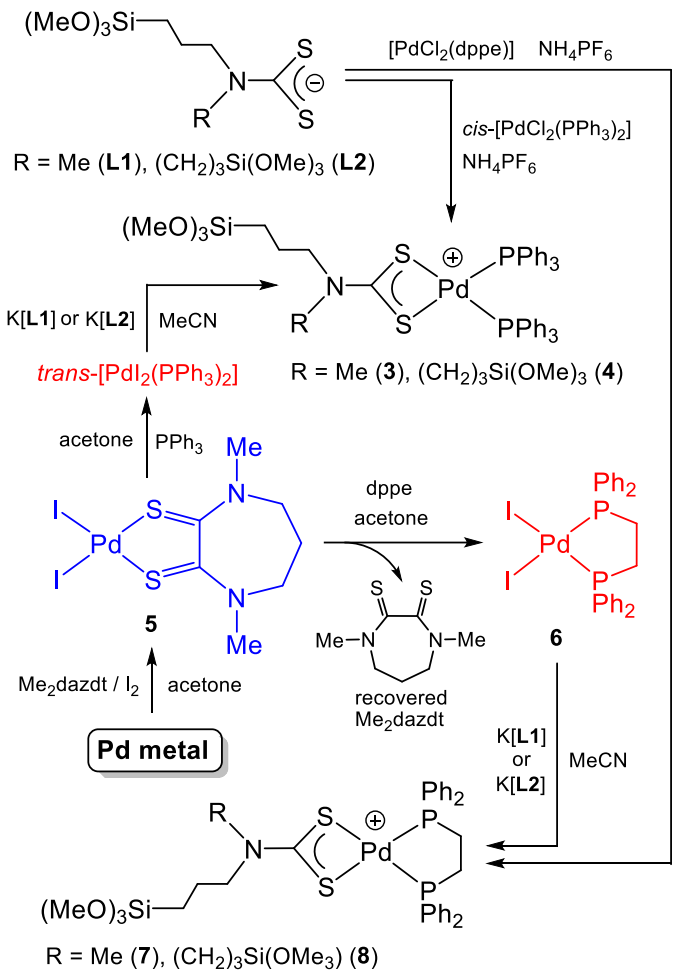

Scheme 3. Synthesis of dithiocarbamate Pd(II) complexes from *cis*-[$PdCl_2(PPh_3)_2$] and from the Pd recovery compound, [$PdI_2(Me_2dazdt)$] (5); dppe = 1,2-bis(diphenylphosphino)ethane.

The overall composition was confirmed by mass spectrometry, which revealed high abundance molecular ions at *m/z* 898 (**3**) and *m/z* 1047 (**4**). Finally, suitable single crystals of both complexes were grown to allow structural characterization by X-ray crystallography. Figures 1 and 2 show the molecular structure of **3** and **4** respectively (see Supporting Information for further structural data). The structures reveal a square planar arrangement at the palladium centers, as would be expected for Pd(II) centers. The two phosphine ligands are accommodated with the phenyl substituents orientated to minimize steric interactions. The bond lengths and angles are similar to related Pd(II) dithiocarbamate compounds, such as $[(dppm)_2Ru(S_2CNC_4H_8NCS_2)Pd(PPh_3)_2](BF_4)_2$ [29] or $[(dppf)Pd(S_2CNC_4H_8NCS_2)Pd(dppf)]^{2+}$ (dppf = 1,1'-diphenylphosphinoferrocene).[30]

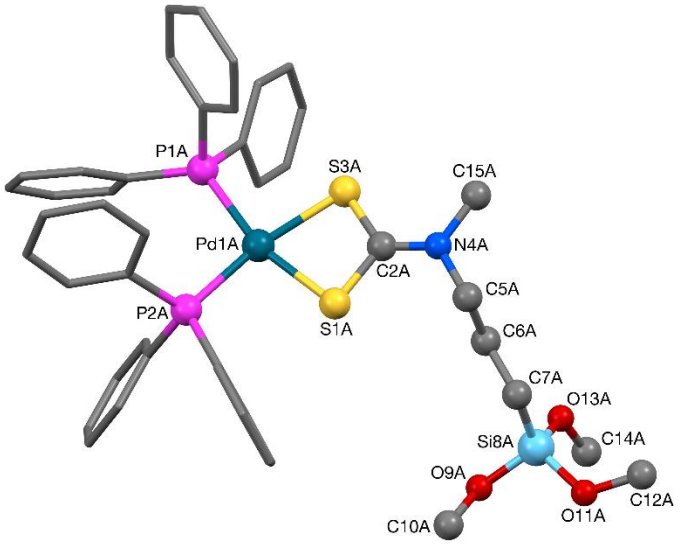

Figure 1. The crystal structure of one (**3-A**) of the two independent cationic complexes present in the crystal of **3**. The PF_6^- counter-ion is omitted.

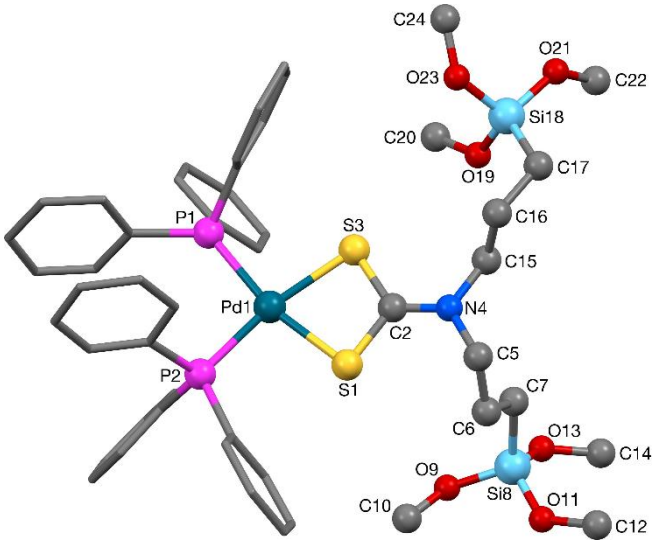

Figure 2. Crystal structure of complex **4**. The PF_6^- counter-ion is omitted.

In order to provide examples with diphosphine ligands, complexes **7** and **8** were prepared using the precursor [$PdCl_2$(dppe)] as shown in Scheme 3. [$PdCl_2$(dppe)] was prepared according to a literature route from the reaction of K_2PdCl_4 with dppe in the presence of HCl.[31,32] The products **7** and **8** were principally characterized by ^{1}H, ^{13}C{^{1}H} and ^{31}P{^{1}H} NMR spectra. An upfield shift in the proton and the phosphorous peaks was observed as noted for complexes **3** and **4** while ^{13}C{^{1}H} NMR spectroscopy showed the CS_2 carbon nucleus resonating at around 206 ppm. Mass spectrometry (ES +ve mode) showed a molecular ion at *m/z* 774 and *m/z* 922 for **7** and **8**, respectively. An X-

ray diffraction study on well-shaped crystals of **7** further confirmed the overall composition of the compound (Figure 3). The structure again showed a square planar arrangement at the Pd(II) center and typical bond lengths and angles for the dithiocarbamate ligand.[33]

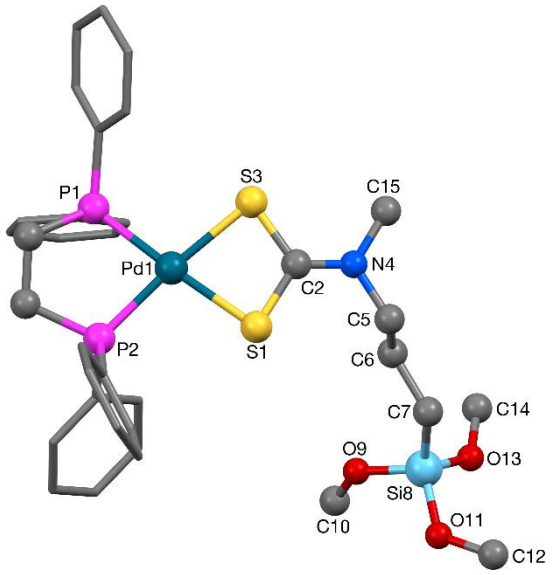

Figure 3. Crystal structure of complex **7**. The PF_6^- counter-ion is omitted.

With the overarching aim to make the process as 'green' as possible, an alternative route was sought, with which to prepare the complexes ahead of their application in catalysis. Our previous research on palladium leaching has promoted the recovery of precious metals from secondary sources (e.g., used automotive catalytic converters) using safe and effective reactants.[19,20] This circular economy approach allows the valorization of recovered products and the preservation of limited natural elemental resources. In particular, as demonstrated and patented by the Deplano group, palladium metal can be easily leached using an organic solution (acetone, methyl ethyl ketone, acetonitrile etc.) of the Me_2dazdt·$2I_2$ adduct in a 1:2 molar ratio under very mild conditions (room temperature and pressure) to produce the homoleptic $[Pd(Me_2dazdt)_2]I_6$ complex as the main product of the reaction.[19] However, the homoleptic nature of this compound precludes the formation of other unsymmetrical compounds through ligand substitution reactions. Based on the successful isolation of the Au(III) compound, $[AuI_2(Me_2dazdt)]^+$,[34] conditions were sought for the effective preparation of the palladium analogue, $[PdI_2(Me_2dazdt)]$ (**5**) by a palladium leaching process. Due to its heteroleptic nature, with two different ligand types displaying different labilities, this compound is an attractive starting point for ligand substitution

reactions. The leaching was conducted in acetone with the Me_2dazdt ligand, iodine and Pd(0) powder in 1:1:1 equivalence (Me_2dazdt/I_2 1:1) as demonstrated in Scheme 3. This reaction gave a high yield (88%) of the black product (**5**) in only a short time (2 h for around 10 mg of Pd powder) and in a very atom-efficient manner, with all the reactants being incorporated into the product. The product was identified as [PdI_2(Me_2dazdt)] (**5**) on the basis of ^{1}H NMR, IR and Raman spectroscopic data. A ν(CN) shift towards higher frequencies was observed for the Me_2dazdt ligand on its coordination to the metal in both the IR (1493 *vs* 1526 cm^{-1}) and Raman (1495 *vs* 1540 cm^{-1}) spectra. The Raman spectrum of **5** also shows the presence of two peaks at 138 and 81 cm^{-1}, which are likely to be due to the Pd-I vibration,[35] while typical peaks for the I_3^- ion are not present. The overall composition was supported by mass spectrometry (*m/z* = 548) and good agreement of elemental analysis with calculated values. The spectroscopic characterization is in full agreement with a structural determination carried out on suitable single crystals using X-ray diffraction techniques. The crystal structure (Figure 4) confirms the square-planar configuration at the Pd(II) and the *S,S*-chelation of the Me_2dazdt ligand with two iodides completing the coordination sphere. It also reveals the presence of an acetone molecule trapped within the coordination sphere of the molecule (Supporting Information). Despite drying the product under vacuum, the presence of this solvate is also indicated in the ^{1}H NMR and IR spectra (2.08 ppm and 1700 cm^{-1}, respectively).

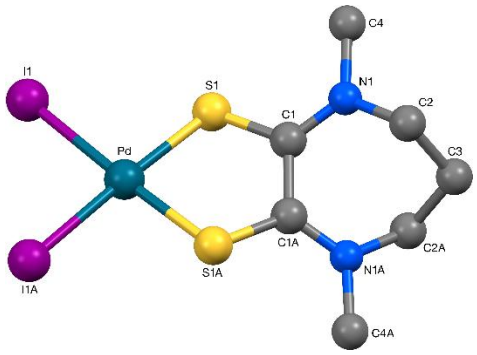

Figure 4. Crystal structure of complex **5**; the complex has C_2 symmetry about an axis that passes through Pd and C3. The acetone molecule in the solvate is not shown.

It is reasonable to assume that the reaction occurs through the formation of Me_2dazdt·I_2 in solution. Similar 1:1 adducts (such as Et_2dazdt·I_2 and Me_2dazdt·IBr) have been isolated in the solid state and characterized previously.[36] This intermediate is a well-established activated species for the Pd(0) leaching process with respect to the free reagents[18,37] and allows the direct formation of two iodide ligands while

simultaneously oxidizing the Pd(0) metal to Pd(II). Compared to the synthesis of the homoleptic product, $[Pd(Me_2dazdt)_2](I_3)_2$, these new leaching conditions utilize less iodine and Me_2dazdt ligand per mole of Pd(0) leached, which is a more sustainable route to recover Pd(0). However, there were concerns that the excess of chelating ligand with respect to the 1:1:1 stoichiometry would lead to a less effective Me_2dazdt/I_2 1:1 leaching system than the standard $Me_2dazdt{\cdot}2I_2$ adduct. When considering further, larger scale application, it is imperative that leaching agents should combine 'greenness' with effectiveness to be sustainable. In order to probe this, a comparison of the two leaching systems was attempted using a calibrated Pd(0) foil in order to perform the reactions under strictly controlled conditions. Heterogeneous phase reactions are heavily affected by a number of different parameters, among them the reactive surface area. Specifically, the Pd dissolution yield was evaluated each hour in terms of weight loss (Δm, mg) of the calibrated foil (0.127 mm thick, 24 mg in mass, 0.23 mmol) using 50 mL of an acetone solution containing either $Me_2dazdt{\cdot}2I_2$ (0.313 g, 0.45 mmol) or the Me_2dazdt/I_2 1:1 mixture (Me_2dazdt: 0.042 g, 0.23 mmol; I_2: 0.057 g, 0.23 mmol). Figure 5 summarizes the results obtained from the different systems at room temperature and, in the case of the 1:1 Me_2dazdt/I_2 mixture, also at the solvent boiling point (60 °C). As expected, under the same conditions (room temperature) the use of $Me_2dazdt{\cdot}2I_2$ makes the process more efficient compared to the 1:1 Me_2dazdt/I_2 system. The plots in Figure 5 show a more dramatic increase in the early stages of the process, which is more pronounced in the case of the $Me_2dazdt{\cdot}2I_2$ system. However, from the fourth hour of reaction, especially in the case of the 1:1 Me_2dazdt/I_2 system, the dissolution rate slows markedly, probably due to the formation of a coating of PdI_2, which hampers further reaction. The effect of raising the temperature on the leaching efficiency was then investigated.

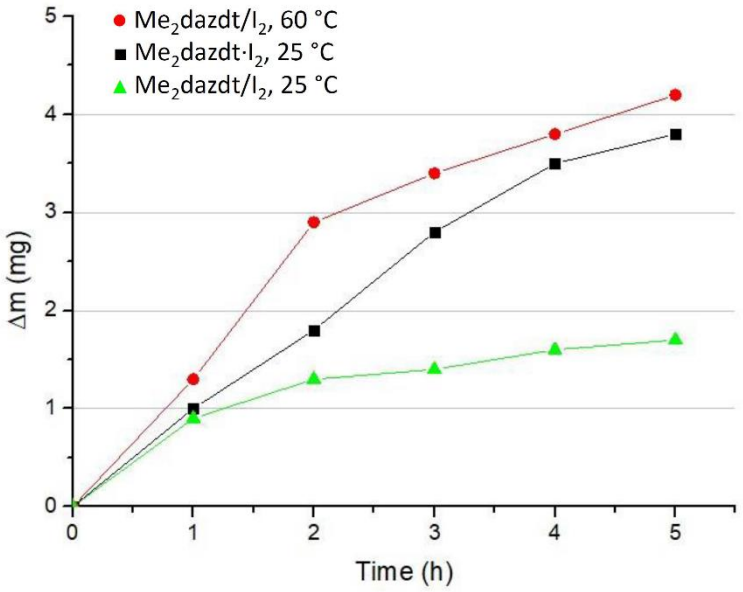

Figure 5. Performance of the leaching process expressed in terms of weight loss (mg) of the Pd foil over time (h) in acetone with the 1:1 Me_2dazdt/I_2 leaching mixture at 25 and 60 °C and with Me_2dazdt·$2I_2$ at room temperature.

As expected, working at the refluxing temperature of the solvent (acetone, 56 °C) led to an increase in the effectiveness of the reaction, achieving a dissolution yield for the 1:1 Me_2dazdt/I_2 system that is higher than that achieved by Me_2dazdt·$2I_2$ at room temperature. This successful result indicated that the process used to form [PdI_2(Me_2dazdt)] (**5**) was still effective when compared with that based on the use of the diiodine adduct. This finding agreed with results obtained by performing the reaction on metal powder, which provided only slightly lower yields within a similar timeframe (2h) using Me_2dazdt/I_2 (88% vs almost quantitative). While these experiments do not claim to address all aspects of the leaching process on real samples (which is beyond the scope of the present work), they do reveal the Me_2dazdt/I_2 mixture to be a very promising, atom-economical and 'green' leaching system. For this reason, the heteroleptic recovery product [PdI_2(Me_2dazdt)] (**5**) was used as the starting point for ligand exchange reactions aimed at producing **3**, **4**, **7** and **8** from this source of recycled palladium. The first attempts to selectively exchange iodide or Me_2dazdt ligands in acetone by the functionalized dithiocarbamate ligand K[**L2**], were unsuccessful due to the formation, in every case, of the very stable homoleptic compound, [Pd(**L2**)$_2$], even when using a 1:1 molar ratio between complex **5** and ligand **L2** (the remainder of the material was unreacted **5**). More satisfactory results were obtained by treating **5** with PPh_3 and dppe as summarized in Scheme 4.

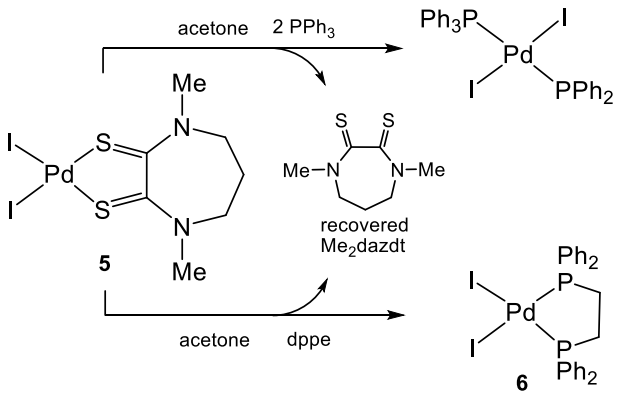

Scheme 4. Ligand exchange reactions between complex **5** and PPh_3 (1:2 ratio) or dppe (1:1 ratio) in acetone or $CHCl_3$ at room temperature. The Me_2dazdt ligand can be recovered at the end of the reaction.

The reactions occurred readily under very mild conditions. The two complexes *trans*-[$PdI_2(PPh_3)_2$] and [PdI_2(dppe)] were isolated in high yield (95 and 87%, respectively). Characterization by IR, ^{1}H and ^{31}P{^{1}H} NMR spectroscopy revealed these data to be identical to that reported in the literature.[38,39] Furthermore, single crystals were grown of *trans*-[$PdI_2(PPh_3)_2$] by vapor diffusion of Et_2O onto a $CHCl_3$ solution of the compound. Measurements of the unit cell showed the crystals to be identical to the previously determined structure of *trans*-[$PdI_2(PPh_3)_2$]·$CHCl_3$.[38] The formation of the *trans* isomer of the complex is noteworthy as the loss of the bidentate Me_2dazdt leaving group would suggest a *cis*-conformation for the final product. However, it is likely that it is the steric requirements of the iodide ligands that ensure that the molecule adopts a *trans* position.

Having established the success of the ligand substitution reactions based on the product (**5**) obtained directly from the recovery of palladium from secondary sources, *trans*-[$PdI_2(PPh_3)_2$] and [PdI_2(dppe)] were used as sustainable precursors for the compounds to be tested in catalysis. It was found that complexes **3** and **4** could be synthesized in high yields (77 and 68%) by treating *trans*-[$PdI_2(PPh_3)_2$] with **1** and **2**, respectively, in the presence of PPh_3 and NH_4PF_6. Similarly, **7** and **8** were prepared by allowing [PdI_2(dppe)] to react with **1** and **2** in the presence of NH_4PF_6. However, in these cases, the low yields of 22 and 35%, respectively, suggest the presence of competitive equilibria or by-product formation. In particular, the formation of the previously reported[40] and very stable $[Pd(dppe)_2]^{2+}$ complex is supported by the experimental evidence achieved when an excess of dppe is added to **5**.

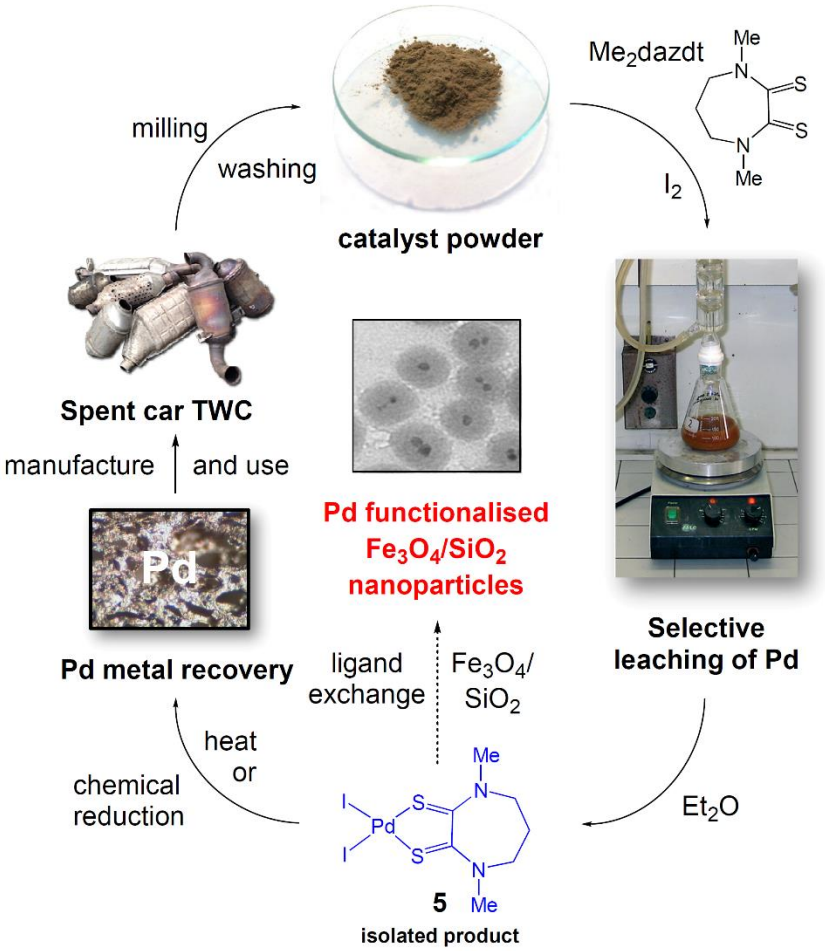

Figure 6. Schematic representation of a postulated circular economy model for the synthesis of a magnetically recoverable catalyst system.

These findings are important in supporting our circular economy model based on palladium recovery from secondary sources and its direct reuse as a valuable precursor to catalytically active Pd(II) complexes and their immobilization on a magnetically recoverable support (Figure 6). The next step was to explore this activity both under homogeneous conditions and as part of a heterogenized magnetically recoverable catalyst system.

Catalytic activity of non-immobilized complexes. Before exploring their immobilization, the catalytic potential of the silyl-functionalized palladium compounds were assessed in the benchmark C–H functionalization of benzo[*h*]quinoline to 10-methoxybenzo[*h*]quinoline (Scheme 1). Such chelate-directed reactions are proposed to proceed through the Pd(II) catalyst first undergoing cyclopalladation whereby Pd(II)

is oxidized to Pd(IV), followed by reductive elimination to yield the product.[11] More recently, bimetallic Pd(III) complexes have also been proposed in such palladium-catalysed carbon–heteroatom bond forming reactions.[41] While a mechanistic study is beyond the scope of this contribution, the behavior demonstrated here parallels that found previously.[10,11,41] Complexes **3**, **4**, **7** and **8** were tested as catalysts under purely homogeneous conditions. Initial experiments were conducted in MeOH with **3** and **4** as catalysts at 100 °C and a loading of 1 mol%, closely following the conditions used by Sanford and co-workers.[11] The transformations were then repeated at 50 °C by optimizing the reaction conditions (loading and times) to achieve satisfactory yields within an acceptable timeframe. The yields of the reaction were determined by ^{1}H NMR spectroscopic analysis of three independent experiments (Section S4 in Supporting Information). Under the conditions reported in the literature, it was found that **3** and **4** both gave yields of 10-methoxybenzo[*h*]quinoline of 85% in 2 hrs. This compared well to the 95% yield achieved in 22 hours by the conventional $Pd(OAc)_2$ pre-catalyst. In order to address concerns regarding the heating of a closed vessel at 100 °C with a solvent that boils at 65 °C, the reaction temperature was set at 50 °C. Figure 7 shows the dependence of the yield with the time of the reaction when the Pd(II) loading is fixed to 1 mol% at 50 °C.

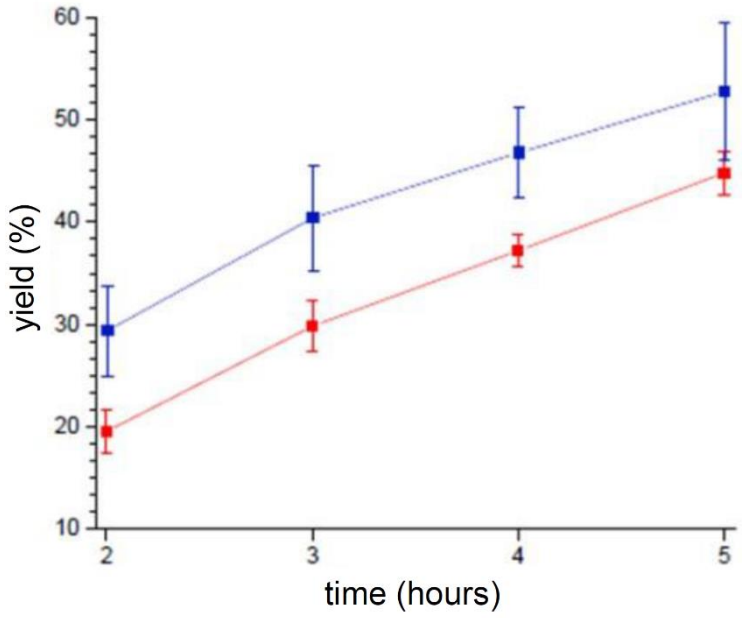

Figure 7. Time dependence of the conversion of benzo[*h*]quinoline to 10-methoxybenzo[*h*]quinoline with **3** (■) and **4** (■) at 1 mol% loading in the presence of $PhI(OAc)_2$ in MeOH at 50 °C.

With a loading of 1 mol%, the initial experiments at 50 °C gave yields of only 29% (with **3**) and 20% (with **4**) after 2 hours. As expected, increasing the duration to 5 hours resulted in around twice the yield. While a further improvement could be expected over extended reaction times, it was decided to explore the impact of increasing the catalyst loading (Figure 8). This demonstrated that a loading of 3 mol% allowed a good yield (around 90%) to be obtained in 2 hours at only 50 °C. Moreover, an increase in the catalyst loading beyond this amount of Pd(II) complex did not lead to a significant improvement. Hence, these conditions were chosen as the optimum for the reaction.

This set of conditions was then used to probe the dppe complexes, **7** and **8**, as catalysts in the same reaction. However, these complexes gave no observable conversion of benzo[*h*]quinoline to 10-methoxybenzo[*h*]quinoline and $^{31}P\{^{1}H\}$ NMR analysis following the reaction showed that the palladium catalysts were unchanged.

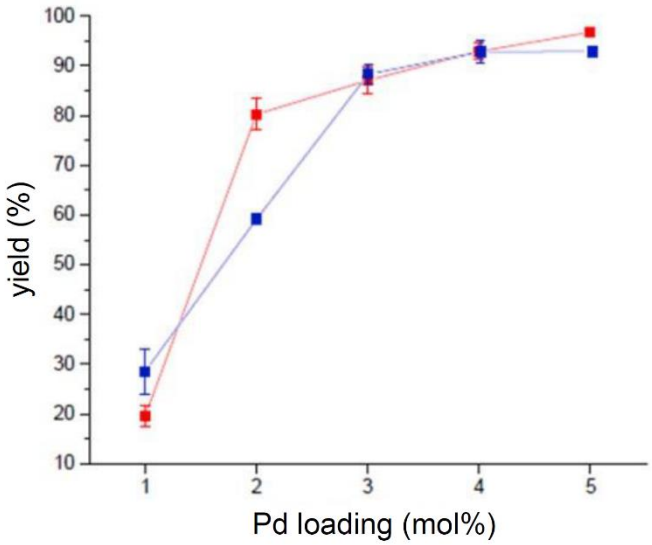

Figure 8. Relationship between catalyst loading and yield of 10-methoxybenzo[*h*]quinoline from benzo[*h*]quinoline using **3** (■) and **4** (■) as catalysts and $PhI(OAc)_2$ as oxidant in MeOH at 50 °C for 2 hours. Values are the average of 3 independent experiments.

These results shed light on certain mechanistic aspects of the catalytic reaction. Since there was no apparent reaction observed with diphosphine compounds **7** or **8**, compared to those with monophosphines (**3** and **4**), the lability of the phosphine ligand must play a key role in the catalysis, suggesting that the dithiocarbamate ligand remains coordinated to the metal center throughout. The electronic and steric properties of dppe and PPh_3 are relatively similar with the exception of the robust, 5-

membered chelate formed by dppe with the palladium center. On the basis of these results, only **3** and **4** were chosen for investigation of the effect of their immobilization on the surface of nanoparticles.

Synthesis and application of functionalized nanoparticles. The synthesis of silica nanoparticles was performed using the well-known Stöber process[42] as described by Kim and coworkers.[43] followed by characterization by transmission electron microscopy (TEM) and IR spectroscopy (Supporting Information). This produced spherical silica nanoparticles with an average diameter of 201 ± 40 nm, which displayed the expected Si-O-Si vibrational mode at 1060 cm^{-1} in the IR spectrum.[42] The synthesis of Fe_3O_4 was performed as described by Rossi et al. via the co-precipitation method with Fe^{2+} and Fe^{3+} precursors.[44] The resulting black precipitate was treated with oleic acid and heated. After further manipulation, the product was obtained as small black nanoparticles (8.0 ± 3.0nm) in a suitable, finely-divided form. In addition to TEM data, IR spectroscopy displayed the expected Fe-O vibrational mode in the 560-600 cm^{-1} range, confirming the synthesis of Fe_3O_4 nanoparticles.[45] This material was coated with a silica shell according to a literature route using tetraethoxy orthosilicate.[46] The resulting brown powder of silica-coated magnetic iron oxide nanoparticles (SiO_2@Fe_3O_4 NP) was collected and dried under vacuum and characterized by IR spectroscopy to features attributable to Fe_3O_4 (560–600 cm^{-1}) and SiO_2 (1060 cm^{-1}). The Fe_3O_4 encapsulation within SiO_2 shells was finally demonstrated by TEM images, where almost spherical particles (average size: 41.0 ± 4.3 nm) were obtained which encapsulated one or more Fe_3O_4 nanoparticles within their cores (Figure S3-2 in Supporting Information).

Functionalisation of core-shell nanoparticles with Pd(II) catalytic units. A schematic representation of the surface functionalization of magnetic nanoparticles with the Pd(II) surface units **3** and **4 i**s shown in Figure 9. Under an inert, dinitrogen atmosphere, 100 mg of SiO_2@Fe_3O_4 NP were treated with **3** (100 mg, 0.10 mmol) or **4** (100 mg, 0.08 mmol) in toluene or $CHCl_3$ (8 mL) and refluxed overnight.

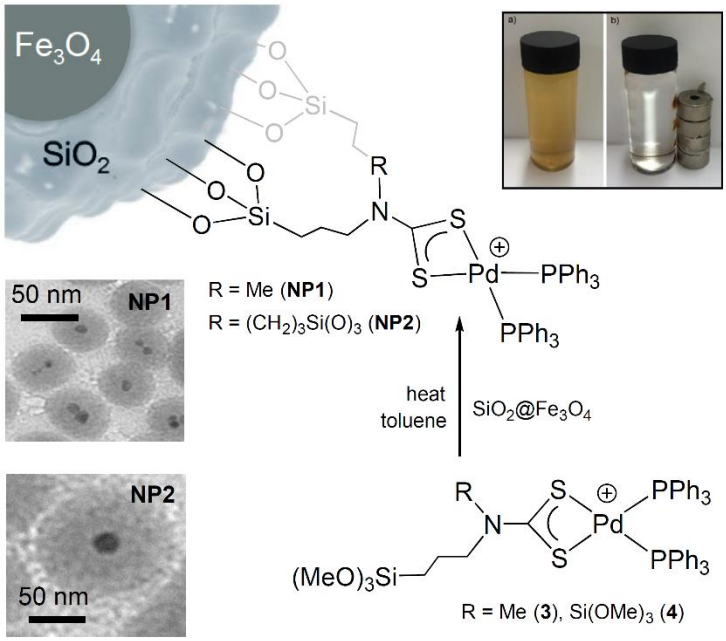

Figure 9. Schematic representation of the preparation of magnetic nanoparticles with Pd(II) surface units with TEM images of the nanoparticles formed and the effect of a hand held magnet on the magnetic material.

The resulting precipitate (of **NP1** or **NP2**) was washed with chloroform to remove unattached surface units and then separated from the liquid through the application of a hand-held magnet (Figure 9). The washing process was repeated 10 times and the washing solution collected (Figure S3-5 in Supporting Information) and analyzed by $^{31}P\{^{1}H\}$ NMR spectroscopy after each wash until no further complex could be observed. The brown solid was dried under vacuum. In order to study the attachment of **3** and **4** to the $SiO_2@Fe_3O_4$ nanoparticles, the materials obtained were studied by TEM, IR spectroscopy and thermogravimetric analysis (TGA). The palladium loading on the surface was analyzed by inductively-coupled plasma optical emission spectroscopy (ICP-OES) after sample digestion. TEM images (Figure 9) clearly show the Fe_3O_4 magnetic core and the SiO_2 coating but are unable to indicate the surface groups, which were instead identified by typical infrared absorptions similar to those found in the unattached compounds **3** and **4**. TGA measurements showed mass loss starting from around 200-250 °C for both **NP1** and **NP2**, confirming the stability of the immobilized system at the temperatures used in the catalytic conditions (up to 100 °C). Overall a loss of around 20-30% of the total mass was observed, which was attributed to the loss of the surface units (Figure 10).

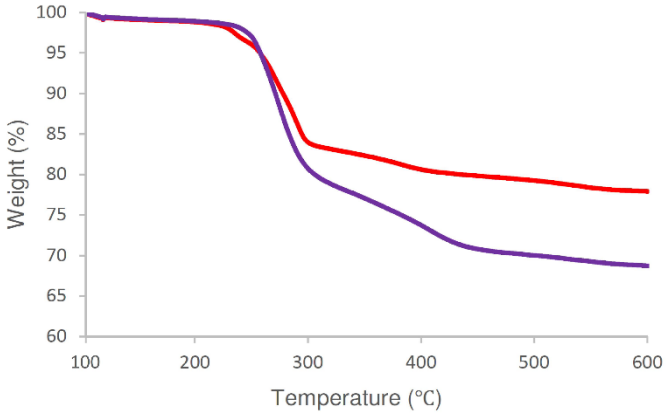

Figure 10. TGA measurements for **3**@SiO_2@Fe_3O_4 (**NP1**) in red and **4**@SiO_2@Fe_3O_4 (**NP2**) in purple.

Due to the variable composition of the iron oxide core and silica shell, this mass loss could not be used to determine the number of surface units with any accuracy. Hence, the functionalized nanoparticles were analyzed first by EDX to confirm the presence of palladium and then by ICP-OES to reveal a palladium loading of 9.0% (**NP1**) and 10.0% (**NP2**) due to the presence of **3** and **4**, respectively, on the surface.

Catalysis with the immobilized palladium-catalyst system. The experiments were performed using the oxidative functionalization of benzo[*h*]quinoline with methanol (Reaction A, Scheme 1) as a benchmark with a 3 mol% Pd loading for 2 hours at 50 °C. After each run, **NP1** and **NP2** were recovered using a hand-held magnet and the nanoparticles used to repeat the reaction with fresh substrates at least a further two times under the same conditions (Table 1).

Table 1. Catalytic results for the reaction of benzo[*h*]quinoline with methanol in the presence of $PhI(OAc)_2$ using a Pd loading of 3 mol% at 50 °C.

	Time (h)	Run 1	Run 2	Run 3	Run 4
Compound **3**	2	87%	-	-	-
Compound **4**	2	88%	-	-	-
3@SiO_2@Fe_3O_4 (**NP1**)	2	32%	13%	5%	-
4@SiO_2@Fe_3O_4 (**NP2**)	2	32%	27%	10%	6%
3@SiO_2@Fe_3O_4 (**NP1**)	22	76%	-	-	-

For runs 2-4, the catalyst material was captured on the side of the flask by a hand-held magnet and washed before recharging with fresh substrate and reactants.

For runs 2-4, the catalyst material was captured on the side of the flask by a hand-held magnet and washed before recharging with fresh substrate and reactants. The results for **NP1** and **NP2** from run 1 showed a significant loss in catalytic effectiveness (about 55% less) when compared with the activity of molecular **3** and **4** under the same conditions, but in the homogeneous phase. This could be due to several factors: (1) the nanoparticles are not as well dispersed as the free molecular units, (2) the insolubility of the nanoparticles meant lower accessibility of the substrate molecules to the catalyst units and (3) the partial decomposition (observed in the tests) caused by mechanical stirring makes them less able to take part in the reaction.

Contrary to expectations, the outward orientation of active sites on the palladium centers (caused by loss of one or more phosphines) on the nanoparticles did not lead to an improvement in the catalytic activity. This could in theory be offset by using a higher catalyst loading, which would be recovered through the facile separation of the catalyst using a hand-held magnet. However, as shown in Table 1, the catalytic activity of recovered **NP1** and **NP2** decreased after each run, becoming ineffective after the third and fourth run for **NP3** and **NP4**, respectively. Additionally, $^{31}P\{^{1}H\}$ NMR analysis of the decanted solution revealed that some of the molecular catalysts (around 30 ppm) had leached into the solution suggesting partial detachment of the catalyst from the surface. Post catalysis ICP-OES analysis of **NP2** supported this finding giving a palladium loading of 2.8%, which is indicative of the loss of surface units. In order to improve the yield from the reaction, it was performed over an extended reaction time. Using a fresh batch of immobilized catalyst system **NP2**, the reaction was carried out for 22 hours (keeping the 3 mol% loading and 50 °C constant), which resulted in a much improved 76% yield of 10-methoxybenzo*[h]*quinoline. Despite the more satisfactory conversion, it was still lower than that obtained using the free molecular catalyst **3**, suggesting that immobilizing the palladium unit on the surface leads to a reduction in its catalytic ability.

Conclusions

An attractive solution to the need to secure sources of palladium for use in its many applications is to recover it from waste material, such as spent automotive catalytic converters. Until recently, this has proved problematic due to the high energy cost of recycling such sources to produce the recovered palladium in metallic or salt form. This contribution illustrates how a mild, safe, low-energy and 100% atom-economical route can be used to generate an the molecular recovery product, $[PdI_2(Me_2dazdt)]$ (**5**), which can be transformed into useful compounds such as *trans*-$[PdI_2(PPh_3)_2]$ or $[PdI_2(dppe)]$ through high-yielding ligand exchange

reactions. Further reaction of these complexes with dithiocarbamate ligands generates active catalysts for the C-H oxidative functionalization reactions, which are equal to the activity of established catalysts[11-13] under milder conditions and shorter timeframes. This was illustrated using the conversion of benzo[*h*]quinoline to 10-methoxybenzo[*h*]quinoline as a benchmark reaction. Furthermore, the reaction of *trans*-[$PdI_2(PPh_3)_2$] with trimethoxysilyl-functionalized dithiocarbamate ligands allows the palladium units to be attached to the surface of iron oxide coated with a silica shell, allowing simple separation using a hand-held magnet. Surprisingly, the catalytic activity of these nanomaterials under heterogeneous conditions was lower than the unattached molecular complexes at the same loading. However, good yields of the product were achieved, albeit requiring extended reaction times, acting as proof of concept for this catalytic approach. In order to improve the recycling of the immobilized catalyst, and to make the proposed circular economy model even more appealing, further effort is needed to improve the synthetic procedure.

The research presented here describes significant innovations to facilitate many of the key steps needed to transform secondary sources of palladium into new molecular and nanoscale catalyst systems. These include (i) the efficient, atom-economical leaching of palladium metal to form a molecular product, [$PdI_2(Me_2dazdt)$] (**5**), (ii) the chemoselective modification of **5** to add bifunctional ligands, (iii) the demonstration of the catalytic activity of the resultant complexes and (iv) the immobilization of these catalytic units onto the surface of a magnetically-recoverable support. The approach of using recovered palladium units to functionalize the surface of core-shell nanoparticles is currently being explored using other attachment methodologies.

Associated content

Supporting Information is available free of charge at X. Contents include the synthetic procedures and characterization with selected spectra and analytical data, including crystallographic data.

Author information

Corresponding Authors

James D. E. T. Wilton-Ely, E-mail: j.wilton-ely@imperial.ac.uk

Angela Serpe, E-mail: serpe@unica.it

Notes

The authors have no conflicts to declare.

Acknowledgements

K.A.J. would like to thank the Ministry of Higher Education, Malaysia for a scholarship on the IPTA Academic Training Scheme and for an Academic Staff Scholarship from the Universiti Teknologi MARA, Malaysia. J.D.E.T.W.-E. and A.S. gratefully acknowledge the support of the Department of Chemistry, Imperial College London and the University of Cagliari for her stay in London. J.D.E.T.W.-E. and A.S. thank the Imperial College European Partners Fund for travel funds. Prof. Carlo Ricci, Department of Physics, University of Cagliari, is gratefully acknowledged for Raman measurements.

References

(1) European Commission - Environment. Available at: http://ec.europa.eu/environment/index_en.htm. (Accessed: 21st August 2018)

(2) Sheldon, R. A.; Arends, I.; Hanefeld, U. *Green Chemistry and Catalysis*, 2007, Wiley-VCH Verlag GmbH & Co. KGaA, Weinheim, Germany; ISBN: 978-3-527-30715-9.

(3) National Research Council (US) Chemical Sciences Roundtable. The Role of the Chemical Sciences in Finding Alternatives to Critical Resources: A Workshop Summary. Washington (DC): National Academies Press (US); 2012. 4, Replacing Critical Materials with Abundant Materials. Available from: https://www.ncbi.nlm.nih.gov/books/NBK100035/ (Accessed: 21 August 2018)

(4) Yin, L.; Liebscher J. Carbon−Carbon Coupling Reactions Catalyzed by Heterogeneous Palladium Catalysts. *Chem. Rev.* **2007**, *107* (1), 133-173, DOI 10.1021/cr0505674 and references cited therein.

(5) Xue, T.; Lin, Z.; Chiu, C.-Y.; Li, Y; Ruan, L.; Wang, G.; Zhao, Z.; Lee, C.; Duan, X., Huang, Y. Molecular Ligand Modulation of Palladium Nanocatalysts for Highly Efficient and Robust Heterogeneous Oxidation of Cyclohexenone to Phenol. *Sci. Adv.* **2017**, *3* (1), e1600615, DOI 10.1126/sciadv.1600615.

(6) Cano, R.; Schmidt, A. F,; McGlacken, G. P. Direct Arylation and Heterogeneous Catalysis; Ever the Twain Shall Meet. *Chem. Sci.* **2015**, *6* (10), 5338-5346, DOI 10.1039/C5SC01534K.

(7) *Cowley, A. Johnson Matthey PGM Market Report, February 2019:* http://www.platinum.matthey.com/documents/new-

item/pgm%20market%20reports/pgm_market_report_february_2019.pdf (Accessed: 20 May 2019).

(8) Karimi, B.; Mansouri, F.; Mirzaei, H. M. Recent Applications of Magnetically Recoverable Nanocatalysts in C-C and C-X Coupling Reactions. *ChemCatChem*. **2015**, *7*(12), 1736-1789, DOI 10.1002/cctc.201403057.

(9) Polshettiwar, V.; Luque, R.; Fihri, A.; Zhu, H.; Bouhrara, M.; Basset, J. M. Magnetically Recoverable Nanocatalysts. *Chem. Rev.* **2011**, *111,* (5), 3036-3075, DOI 10.1021/cr100230z.

(10) Champion, M. J.; Solanki, R.; Delaude, L.; White, A. J.; Wilton-Ely, J. D. E. T. Synthesis and Catalytic Application of Palladium Imidazol(in)ium-2-dithiocarboxylate Complexes. *Dalton Trans*. **2012**, *41* (40), 12386-12394, DOI 10.1039/C2DT31413D.

(11) Dick, A. R.; Hull, K. L.; Sanford, M. S. A Highly Selective Catalytic Method for the Oxidative Functionalization of C−H Bonds. *J. Am. Chem. Soc.* **2004**,*126*, (8), 2300-2301, DOI 10.1021/ja031543m.

(12) Lyons, T. W.; Sanford, M. S. Palladium-Catalyzed Ligand-Directed C−H Functionalization Reactions. *Chem. Rev.* **2010**, *110* (2), 1147-1169, DOI 10.1021/cr900184e.

(13) Jantan, K. A.; Kwok, C. Y.; Chan, K. W.; Marchiò, L.; White, A. J. P.; Deplano, P.; Serpe, A.; Wilton-Ely, J. D. E. T. From Recovered Metal Waste to High-Performance Palladium Catalysts. *Green Chem*. **2017**, *19* (24), 5846-5853, DOI 10.1039/C7GC02678A.

(14) Hogarth, G. Transition Metal Dithiocarbamates: 1978–2003. *Prog. Inorg. Chem.* **2005**, *53*, 71-561, DOI 10.1002/0471725587.ch2.

(15) Schierl, R.; Nagel, U.; Beck, W. Reactions of Transition Metal Compounds with Primary Amines and Carbon Disulfide: Dithiocarbimato and Dithiocarbamato Complexes of Palladium, Platinum, Nickel, Cobalt and Gold. X-Ray Structure of $(Et_3P)_2MS_2CNCH_2Ph$ (M= Pd, Pt). *Z. Naturforsch. B* **1984**, *39* (5), 649-660, DOI 10.1515/znb-1984-0520.

(16) Exarchos, G.; Nyburg, S. C.; Robinson, S. D. The Synthesis and Characterisation of $[Pd(S_2CNEt_2)(Ph_2PCH_2CH_2PPh_2]^+$ Salts of Some Chloro- and Bromo-metallate Anions — X-ray Crystal Structures of $[Pd(S_2CNEt_2)(Ph_2PCH_2CH_2PPh_2)^+[MCl_2]^-$ (M = Cu, Ag). *Polyhedron* **1998**, *17* (8), 1257-1266, DOI 10.1016/S0277-5387(97)00386-0.

(17) http://ec.europa.eu/environment/circular-economy/index_en.htm (Accessed: 21st August 2018)

(18) Serpe, A.; Artizzu, F.; Mercuri, M. L.; Pilia, L.; Deplano, P. Charge Transfer Complexes of Dithioxamides with Dihalogens as Powerful Reagents in the Dissolution of Noble Metals. *Coord. Chem. Rev.* **2008**, *252* (10-11), 1200-1212, DOI 10.1016/j.ccr.2008.01.024.

(19) Serpe, A.; Bigoli, F.; Cabras, M. C.; Fornasiero, P.; Graziani, M.; Mercuri, M. L.; Montini, T.; Pilia, L.; Trogu, E. F.; Deplano, P. Pd-Dissolution Through a Mild and Effective One-Step Reaction and its Application for Pd-Recovery from Spent Catalytic Converters. *Chem. Commun.* **2005**, *8*, 1040-1042, DOI 10.1039/B415799K.

(20) Deplano, P.; Mercuri, M. L.; Trogu, E. F.; Serpe, A.; Fornasiero, P.; Graziani, M. European Patent 1743044B1, **2004**.

(21) Ojeda, M. W.; del Carmen Ruiz, M.; Godoy, M. E.; Rivarola, J. B.; Recovery of Palladium from an Exhausted Catalyst by Chlorination: Effect of Carbon Content and Thermal Treatment. *Trans. Inst. Min. Metall., Sect. C*, **1999**, *108*, C33.

(22) Cui, J.; Zhang, L. Metallurgical Recovery of Metals from Electronic Waste: A Review. *J. Hazard. Mater.* **2008**,158 (*2-3*), 228-256, DOI 10.1016/j.jhazmat.2008.02.001.

(23) Cuif, J.-P. US Patent 6455018, **2002**.

(24) Gombac, V.; Montini, T.; Falqui, A.; Loche, D.; Prato, M.; Genovese, A.; Mercuri, M. L.; Serpe, A.; Fornasiero, P.; Deplano, P. From Trash to Resource: Recovered-Pd from Spent Three-Way Catalysts as a Precursor of an Effective Photo-catalyst for H_2 Production. *Green Chem.* **2016**, *18* (9), 2745-2752, DOI 10.1039/C5GC02908B.

(25) Uivarosi, V.; Badea, M.; Aldea, V.; Chirigiu, L.; Olar, R. Thermal and Spectral Studies of Palladium(II) and Platinum(IV) Complexes with Dithiocarbamate Derivatives. *J. Therm. Anal. Calorim.* **2013**, *111* (2), 1177-1182, DOI 10.1007/s10973-012-2315-5.

(26) Khan, S. Z.; Amir, M. K.; Ullah, I.; Aamir, A.; Pezzuto, J. M.; Kondratyuk, T.; Bélanger-Gariepy, F.; Ali, A.; Khan, S. New Heteroleptic Palladium(II) Dithiocarbamates: Synthesis, Characterization, Packing and Anticancer Activity Against Five Different Cancer Cell Lines. *Appl. Organomet. Chem.* **2016**, *30* (6), 392-398, DOI 10.1002/aoc.3445.

(27) Logacheva, N. M.; Baulin, V. E.; Tsivadze, A. Y.; Pyatova, E. N.; Ivanova, I. S.; Velikodny, Y. A.; Chernyshev, V. V.; Ni(II), Co(II),Cu(II), Zn(II) and Na(I) Complexes of a Hybrid Ligand 4′-(4‴-benzo-15-crown-5)-methyloxy-2,2′:6′,2″-Terpyridine. *Dalton Trans.* **2009**, (14), 2482-2489, DOI 10.1039/B819805E.

(28) Daasch L.; Smith, D. Infrared Spectra of Phosphorus Compounds. *Anal. Chem.* **1951**, *23* (6), 853-868, DOI 10.1021/ac60054a008.

(29) Knight, E. R.; Cowley, A. R.; Hogarth, G.; Wilton-Ely, J. D. Bifunctional Dithiocarbamates: A Bridge between Coordination Chemistry and Nanoscale Materials. *Dalton Trans.* **2009** (4), 607-609, DOI 10.1039/B814476A.

(30) Knight, E. R.; Leung, N. H.; Lin, Y. H.; Cowley, A. R.; Watkin, D. J.; Thompson, A. L.; Hogarth, G.; Wilton-Ely, J. D. E. T. Multimetallic Arrays: Symmetrical Bi-, Tri- and Tetrametallic Complexes Based on the Group 10 Metals and the Functionalisation of Gold Nanoparticles with Nickel-Phosphine Surface Units. *Dalton Trans.* **2009** (19), 3688-3697, DOI 10.1039/B821947H.

(31) Sabounchei, S. J.; Ahmadi, M.; Nasri, Z. Five-Membered Cyclopalladated Complex Containing Bidentate Phosphine Ligands; Synthesis, Characterization, and Highly Efficient Suzuki Cross-Coupling Reactions. *J. Coord. Chem.*, **2013**, *66* (3), 411-423, DOI 10.1080/00958972.2012.759216.

(32) Noskowska, M.; Śliwińska, E.; Duczmal, W. Simple Fast Preparation of Neutral Palladium(II) Complexes with $SnCl_3$ and Cl^- ligands. *Transit. Met. Chem.* **2003**, *28* (7), 756-759, DOI 10.1023/A:102606470.

(33) Oliver, K.; White, A. J. P.; Hogarth, G.; Wilton-Ely, J. D. E. T. Multimetallic Complexes of Group 10 and 11 Metals Based on Polydentate Dithiocarbamate Ligands. *Dalton Trans.* **2011**, *40* (22), 5852-5864, DOI 10.1039/C0DT01745K.

(34) Bigoli F.; Pellinghelli, M. A.; Deplano, P.; Mercuri, M. L.; Pintus, G.; Serpe, A.; Trogu, E. F. A Powerful New Oxidation Agent Towards Metallic Gold Powder: *N,N′*-dimethylperhydrodiazepine-2,3-dithione (D) bis(diiodine). Synthesis and X-ray Structure of $[AuDI_2]I_3$. *Chem. Commun.* **1998**, (21), 2351-2352, DOI 10.1039/A806158K.

(35) Nakamoto, K. Infrared and Raman Spectra of Inorganic and Coordination Compounds, 4th edition, John Wiley & Sons, Inc., New York, 1986.

(36) Serpe, A. Innovative Low-Polluting Reagents for Noble-Metals Dissolution and Recovery, PhD Thesis, University of Cagliari, 2003.

(37) Deplano, P.; Ferraro, J. R.; Mercuri, M. L.; Trogu, E. F. Structural and Raman Spectroscopic Studies as Complementary Tools in Elucidating the Nature of the Bonding in Polyiodides and in Donor-I_2 Adducts. *Coord. Chem. Rev.* **1999**, *188* (1), 71-95, DOI 10.1016/S0010-8545(98)00238-0.

(38) Kubota, M.; Ohba, S.; Saito, Y. Structure of *Trans*-diiodobis(triphenylphosphine)palladium(II)–trichloromethane (1/1). *Acta Cryst.* **1991**, *C47*, (8), 1727-1729, DOI 10.1107/S0108270191001956.

(39) Aizawa, S. I.; Majumder, A.; Maeda, D.; Kitamura, A. Mechanism of Catalytic Chalcogen Atom Replacement of Phosphine Chalcogenides and Separation of the Intermediate Phosphine. *Chem. Lett.* **2008**, *38* (1), 18-19, DOI 10.1246/cl.2009.18.

(40) Lassahn, P. G.; Lozan, V.; Wu, B.; Weller, A. S.; Janiak, C. Dihalogeno(diphosphane)metal(II) Complexes (metal = Co, Ni, Pd) as Pre-Catalysts for the Vinyl/Addition Polymerization of Norbornene – Elucidation of the Activation Process with $B(C_6F_5)_3$/$AlEt_3$ or Ag[*closo*-1-$CB_{11}H_{12}$] and Evidence for the *in situ* formation of "naked" Pd^{2+} as a highly active species. *Dalton Trans.* **2003**, (23), 4437-4450, DOI 10.1039/B302937A.

(41) Powers, D. C.; Ritter, T. Bimetallic Pd(III) complexes in palladium-catalysed carbon–heteroatom bond formation. *Nat. Chem.*, **2009**, *1* (4), 302-309, DOI 10.1038/nchem.246.

(42) Stöber, W.; Fink, A.; Bohn, E. Controlled Growth of Monodisperse Silica Spheres in the Micron Size Range. *J. Colloid Interface Sci.* **1968**, *26* (1), 62-69, DOI 10.1016/0021-9797(68)90272-5.

(43) Park, S. K.; Kim, K. D.; Kim, H. T. Preparation of Silica Nanoparticles: Determination of the Optimal Synthesis Conditions for Small and Uniform Particles. *Colloids Surf. A* **2002**, *197* (1-3), 7-17, DOI 10.1016/S0927-7757(01)00683-5.

(44) Rossi, L. M.; Costa, N. J.; Silva, F. P.; Wojcieszak, R. Magnetic Nanomaterials in Catalysis: Advanced Catalysts for Magnetic Separation and Beyond. *Green Chem.* **2014**, *16* (6), 2906-2933, DOI 10.1039/C4GC00164H.

(45) Bordbar, A. K.; Rastegari, A. A.; Amiri, R.; Ranjbakhsh, E.; Abbasi, M.; Khosropour, A. R. Characterization of Modified Magnetite Nanoparticles for Albumin Immobilization, *Biotechnol. Res. Int.*, **2014**, 1–6, DOI 10.1155/2014/705068.

(46) Jacinto, M. J.; Kiyohara, P. K.; Masunaga, S. H.; Jardim, R. F.; Rossi, L. M. Recoverable Rhodium Nanoparticles: Synthesis, Characterization and Catalytic Performance in Hydrogenation Reactions. *Appl. Catal. A* **2008**, *338*, (1-2), 52–57, DOI 10.1016/j.apcata.2007.12.018.

For ToC use:

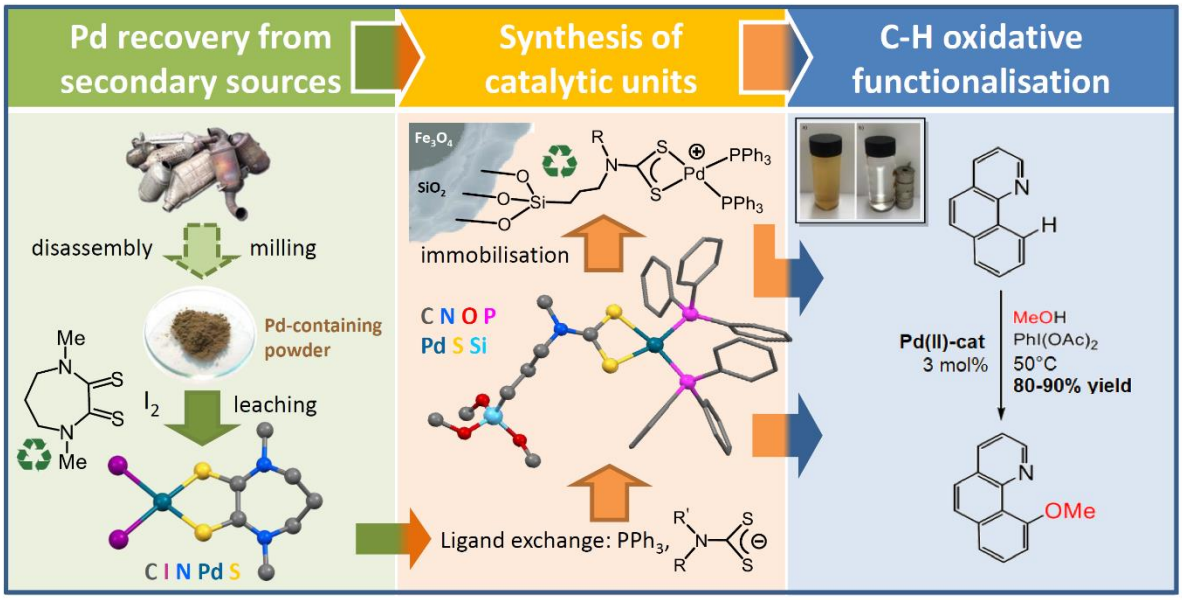

A series of leaching, ligand exchange and immobilisation steps deliver molecular and immobilised catalyst systems derived from palladium waste.

[19 words]

Supporting Information

From recovered palladium to molecular and nanoscale catalysts

Khairil A. Jantan, Kuang Wen Chan, Laura Melis, Andrew J. P. White, Luciano Marchiò, Paola Deplano, Angela Serpe* and James D. E. T. Wilton-Ely*

E-mail: serpe@unica.it
j.wilton-ely@imperial.ac.uk

Total number of Pages: 40
Total number of Figures: 42
Total number of Tables: 6

S1. Experimental

All reagents were used as received. The palladium powder used was >99.9% (<1 micron). All reactions were carried out in the air and with technical solvents without precautions to exclude moisture or oxygen, unless otherwise stated. In cases where anhydrous solvents were used, the anhydrous solvents were dried by passing them through columns of molecular sieves in a solvent purification system. The compounds *cis*-$[PdCl_2(PPh_3)_2]$[S1] and $[PdCl_2(dppe)]$[S2,S3] were prepared using literature procedures. ^{1}H NMR, $^{31}P\{^1H\}$ NMR and $^{13}C\{^1H\}$ NMR spectra were recorded at 25 °C on Varian Mercury 300 and Bruker AV400 spectrometers in $CDCl_3$ unless stated otherwise. All coupling constants are in Hertz. Chemical shifts are reported in ppm with respect to the solvent peak. Attribution of some NMR signals was made using quantitative NMR, HSQC and DEPT-135 experiments. Infrared data were obtained using a Perkin-Elmer Spectrum 100 FT-IR spectrometer. Crystallography data were obtained using the Agilent Xcalibur PX Ultra A diffractometer (Mo) and Agilent Xcalibur 3 E diffractometer (Cu). Thermogravimetric analysis (TGA) was carried out on Mettler Toledo TGA/DSC 1LF/UMX. Mass spectra (MS) were recorded on a Micromass Autospec Premier, Micromass LCT Premier and a VG Platform II spectrometer using the Electrospray ionization (ESI) technique. Elemental analyses (EA) were performed at the London Metropolitan University (UK). Transmission electron microscopy (TEM) images were obtained using a JEOL 2010 high-resolution TEM (80-200 kV) equipped with an Oxford Instruments INCA EDS 80 mm X-Max detector system. The grids used were 300 mesh copper with carbon films. Inductively coupled plasma optical emission spectroscopy (ICP-OES) analyses were performed using a Perkin-Elmer 2000 DV ICP-OES spectrometer. Raman spectra were recorded on a B & W Tek i-Raman EX spectrometer, fitted with an Indium-Gallium-Arsenide detector (room temperature) and operating with an excitation frequency of 1064 nm (Nd:YAG laser). Spectra were acquired on the crude sample in the range 0 - 2500 cm^{-1}.

Ligand synthesis

K[$S_2CN(Me)CH_2CH_2CH_2Si(OMe)_3$] (K[L1])

The starting material, 3-trimethoxysilylpropyl-methylamine (1000 mg, 5.17 mmol), was dissolved in acetonitrile (20 mL) and stirred with K_2CO_3 (2875 mg, 20.68 mmol) for 30 minutes. Carbon disulfide (0.38 mL, 6.20 mmol) was added to the solution and stirring continued for 2 hours. The solution was filtered to remove excess K_2CO_3 and the solvent was removed. The residue was dissolved in chloroform (10 mL) and filtered through diatomaceous earth (Celite). The solvent was removed to give a yellow oily product. Diethyl ether (20 mL) was added and triturated in an ultrasound bath to give a pale yellow solid product. The solid product separated by filtration, washed with diethyl ether (5 mL) and dried under vacuum. Yield: 815 mg (52%). IR (ATR): 2936, 2839, 1461 (vCN), 1267 (vC=S), 1187, 1063, 963 (vC-S), 814, 783 cm^{-1}. ^1H NMR ($CDCl_3$, 400 MHz): δ 0.64 (t, 2H, CH_2, J_{HH} = 8.0 Hz), 1.77 (pent., 2H, CH_2, J_{HH} = 8.0 Hz), 3.47 (s, 3H, NCH_3), 3.55 (s, 9H, OCH_3), 4.02 (m, 2H, CH_2) ppm. $^{13}C\{^1H\}$ NMR ($CDCl_3$, 101 MHz): δ 5.8 (s, CH_2), 19.9 (s, CH_2), 42.6 (s, NCH_3), 50.5 (s, OCH_3), 58.5 (s, CH_2), 210.8 (s, CS_2) ppm. MS (ES +ve) *m/z* (abundance): 268 (100) $[M]^+$. Elem. Anal. Calcd. for $C_8H_{18}KNO_3S_2Si$ (M_W = 307.55): C, 31.2; H, 5.9; N, 4.6%. Found: C, 31.0; H, 6.0; N, 4.5%.

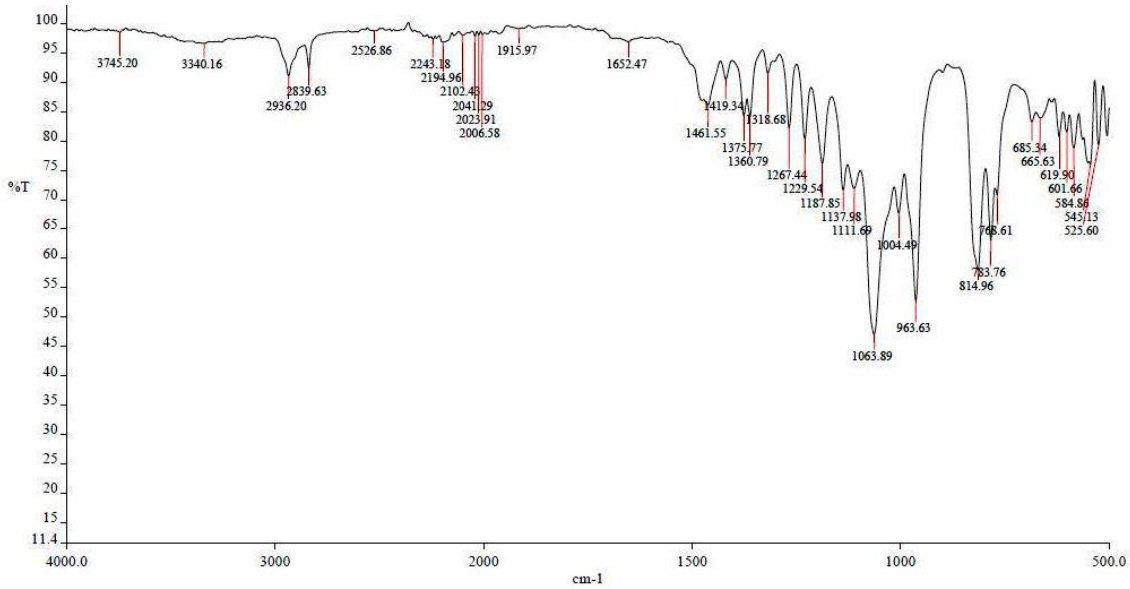

Figure S1-1. Solid state infrared spectrum of K[**L1**].

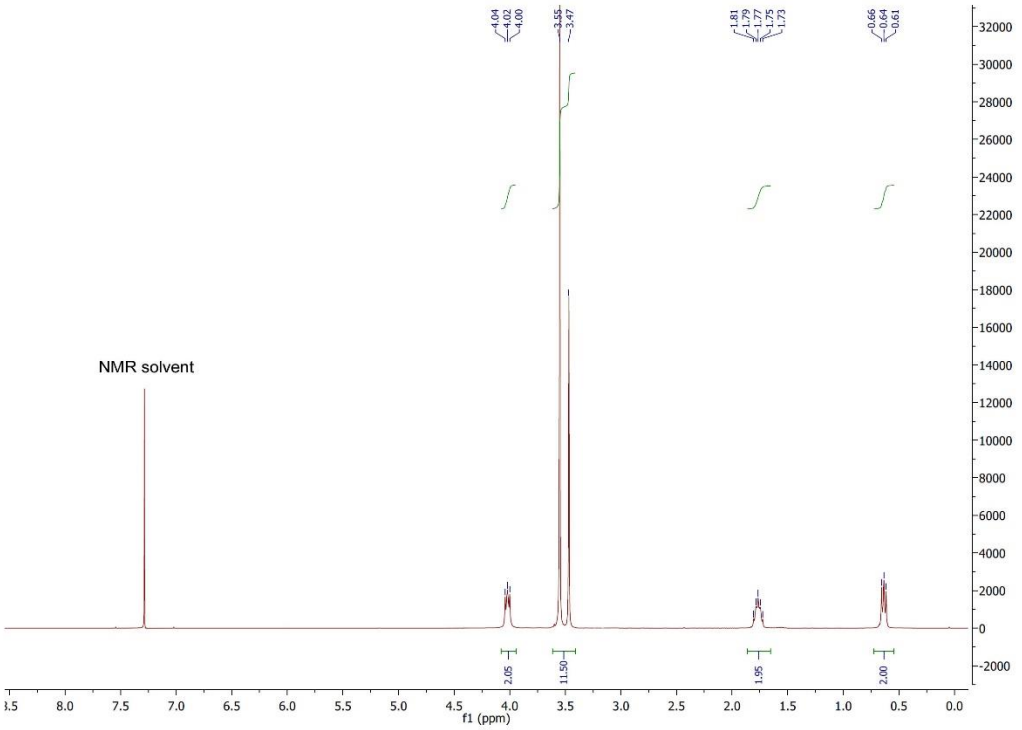

Figure S1-2. ^{1}H NMR spectrum of K[**L1**] in $CDCl_3$.

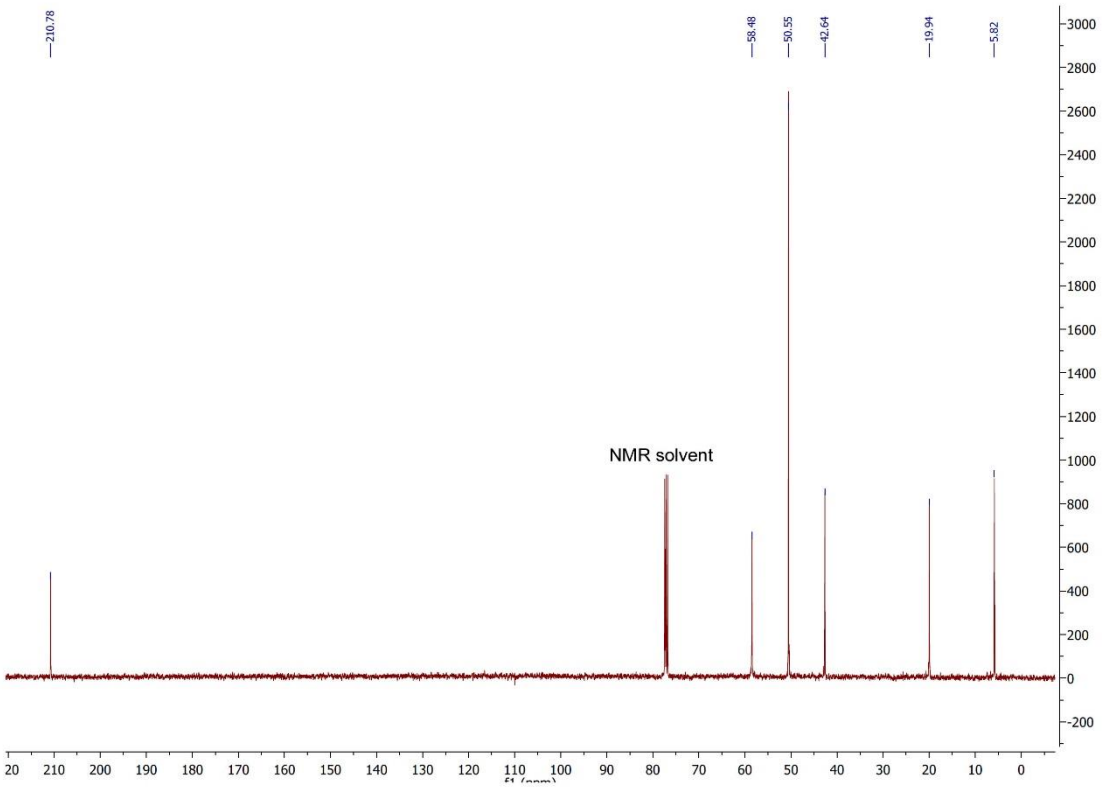

Figure S1-3. $^{13}C\{^{1}H\}$ NMR spectrum of K[**L1**] in $CDCl_3$.

K[$S_2CN\{CH_2CH_2CH_2Si(OMe)_3\}_2$] K[L2]

Bis(trimethoxysilylpropyl)-amine (1000 mg, 2.93 mmol) was dissolved in acetonitrile (20 mL) and stirred with potassium carbonate (1620 mg, 11.72 mmol) for 30 minutes. Carbon disulfide (0.22 mL, 3.52 mmol) was added to the solution and stirring continued for 2 hours. The solution was filtered to remove excess K_2CO_3 and the solvent was removed. The residue was dissolved in $CHCl_3$ (10 mL) and filtered through diatomaceous earth (Celite). The solvent was removed to give a yellow oily product. Et_2O (20 mL) was added and triturated in an ultrasound bath to give a pale yellow solid product. The solid product separated by filtration, washed with Et_2O (5 mL) and dried under vacuum. Yield: 773 mg (58%). IR (ATR): 2939, 2839, 1467 (vCN), 1250 (vC=S), 1191, 1063, 965 (vC-S), 783 cm^{-1}. ^1H NMR ($CDCl_3$, 400 MHz): δ 0.64 (t, 4H, CH_2, J_{HH} = 8.1 Hz), 1.83 (m, 4H, CH_2), 3.58 (s, 18H, OCH_3), 3.96 (t, 4H, CH_2, J_{HH} = 8.1 Hz) ppm. $^{13}C\{^1H\}$ NMR ($CDCl_3$, 101 MHz): δ 6.0 (s, CH_2), 20.0 (s, CH_2), 50.5 (s, OCH_3), 56.2 (s, CH_2), 210.9 (s, CS_2) ppm. MS (ES +ve) *m/z* (abundance): 416 (70) $[M]^+$. Elem. Anal. Calcd. for $C_{13}H_{30}KNO_6S_2Si_2$ (M_w = 455.78): C, 34.3; H, 6.6; N, 3.1 %. Found: C, 34.1; H, 6.7; N, 3.2 %.

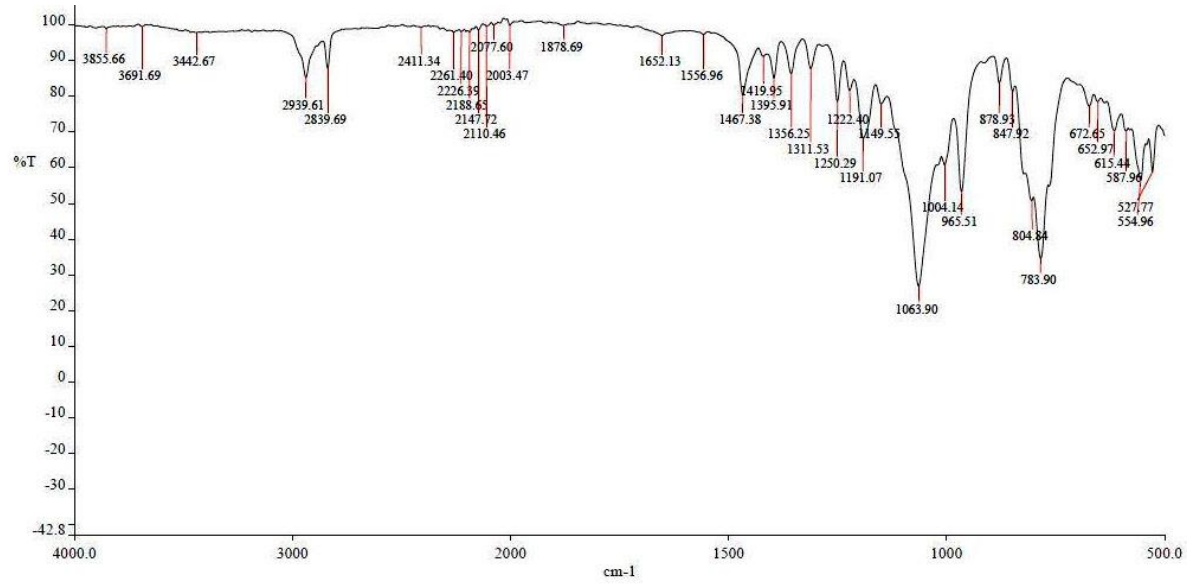

Figure S1-4. Solid state infrared spectrum of K[**L2**].

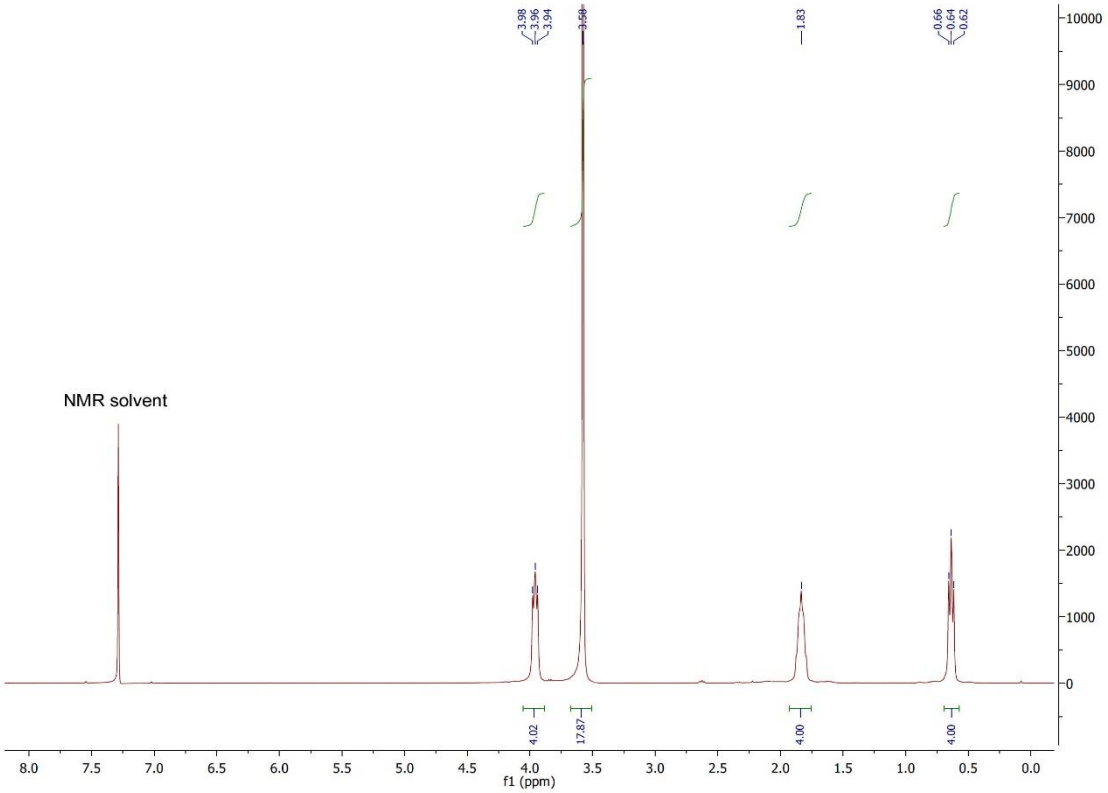

Figure S1-5. ^{1}H NMR spectrum of K[**L2**] in $CDCl_3$.

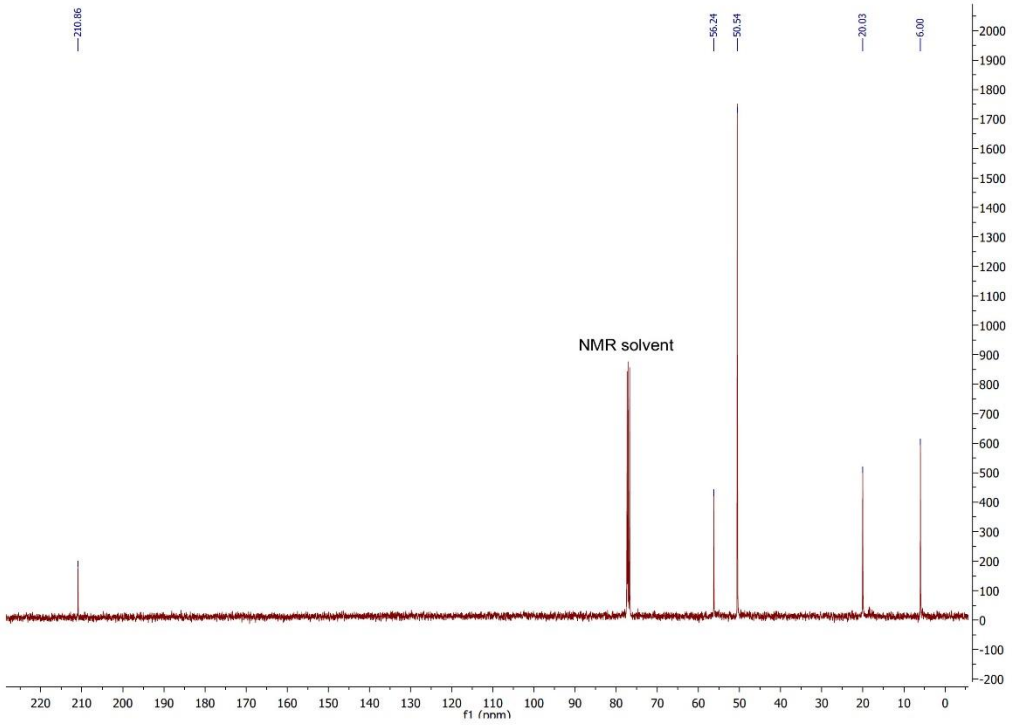

Figure S1-6. $^{13}C\{^{1}H\}$ NMR spectrum of K[**L2**] in $CDCl_3$.

Palladium(II) complexes from commercial precursors

[Pd(L1)(PPh_3)$_2$]PF_6 (3)

a) *cis*-[$PdCl_2(PPh_3)_2$] (500 mg, 0.71 mmol) was dissolved in $CHCl_3$ (10 mL). K[**L1**] (258 mg, 0.81 mmol) was dissolved in MeOH (10 mL). NH_4PF_6 (232 mg, 1.42 mmol) was dissolved in MeOH (5 mL). All three solutions were mixed and refluxed with stirring overnight. The solvent was removed and the residue was dissolved in $CHCl_3$ (20 mL). The solution was filtered through Celite and solvent removed. Et_2O (20 mL) was added and triturated in an ultrasound bath. The yellow solid product separated by filtration, washed with Et_2O (5 mL) and dried under vacuum. Yield: 627 mg (84%). **b)** *trans*-[$PdI_2(PPh_3)_2$] (20 mg, 0.023 mmol), PPh_3 (31.3 mg, 0.138 mmol) and NH_4PF_6 (6.5 mg, 0.046 mmol) were dissolved in acetonitrile (5 mL). K[**L1**] (7.2 mg, 0.024 mmol) was dissolved in acetonitrile (3 mL) and added dropwise into the mixture. The mixture was left to stir overnight. The solution color changed from orange to yellow. The solvent was removed and the residue was dissolved in chloroform (10 mL). The solution was filtered through Celite and solvent removed. Et_2O (1 mL) was added and triturated in an ultrasound bath and left at 4 °C for the product to precipitate. The product is sparingly soluble in Et_2O. The yellow solid product separated by filtration, washed with Et_2O (1 mL) and dried under vacuum. Yield: 18.1 mg (77%). IR (ATR): 2941, 2840, 1480 (vCN), 1261 (vC=S), 1190, 1077, 963 (vC-S), 831 (vPF), 744, 691 cm^{-1}. ^1H NMR ($CDCl_3$, 400 MHz): δ 0.59 (t, 2H, CH_2, J_{HH} = 8.2 Hz), 1.71 (m, 2H, CH_2), 3.21 (s, 3H, N-CH_3), 3.55 (s, 9H, OCH_3), 3.63 (t, 2H, CH_2, J_{HH} = 7.6 Hz), 7.32 - 7.47 (m, 30H, PPh_3) ppm. $^{13}C\{^1H\}$ NMR ($CDCl_3$, 101 MHz): δ = 6.1 (s, CH_2), 20.3 (s, CH_2), 36.6 (s, N-CH_3), 50.7 (s, OCH_3), 53.5 (s, CH_2), 128.9 (m, *o/m*-PC_6H_5), 131.8 (s, *p*-PC_6H_5), 134.0 (*ipso*-PC_6H_5, obscured), 134.1 (m, *o/m*-PC_6H_5), 206.5 (s, CS_2) ppm. $^{31}P\{^1H\}$ NMR ($CDCl_3$, 162 MHz): δ -146.5 (sept., PF_6^-, J_{PC} = 712.4 Hz), 30.3, 30.6 (d x 2, PPh_3, J_{PP} = 35.0 Hz) ppm. MS (ES +ve) *m/z* (abundance): 898 (100) $[M]^+$. Elem. Anal. Calcd. for $C_{44}H_{48}F_6NO_3P_3PdS_2Si$ (M_W = 1044.42): C, 49.4; H, 5.1; N, 1.2%. Found: C, 49.8; H, 4.7; N, 1.4%.

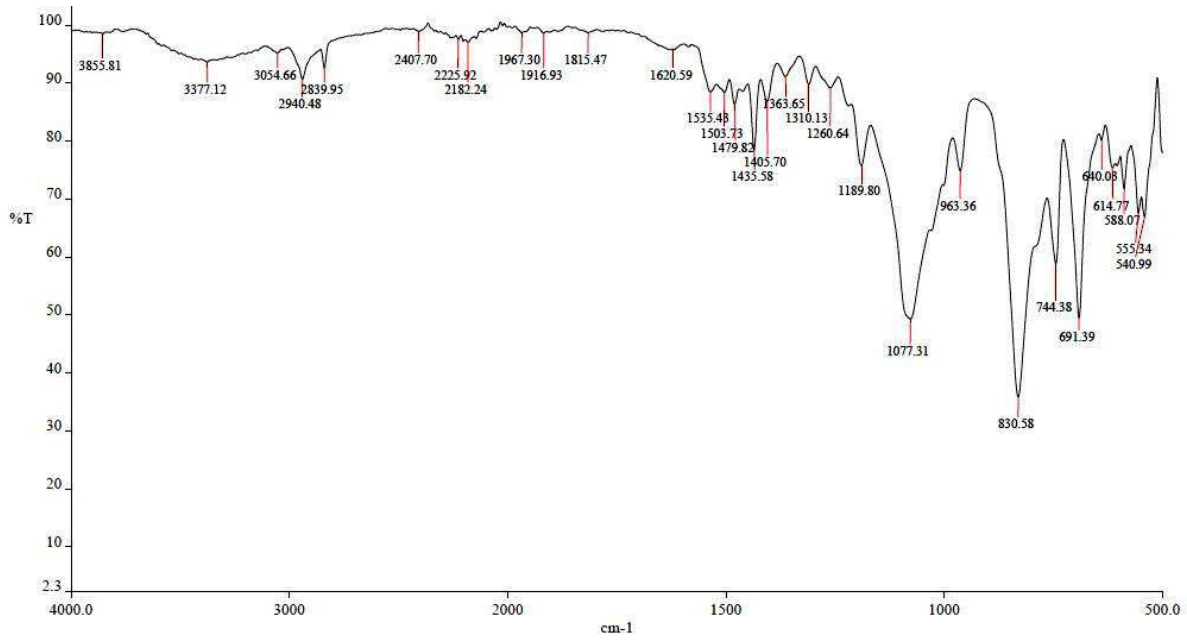

Figure S1-7. Solid state infrared spectrum of **3**.

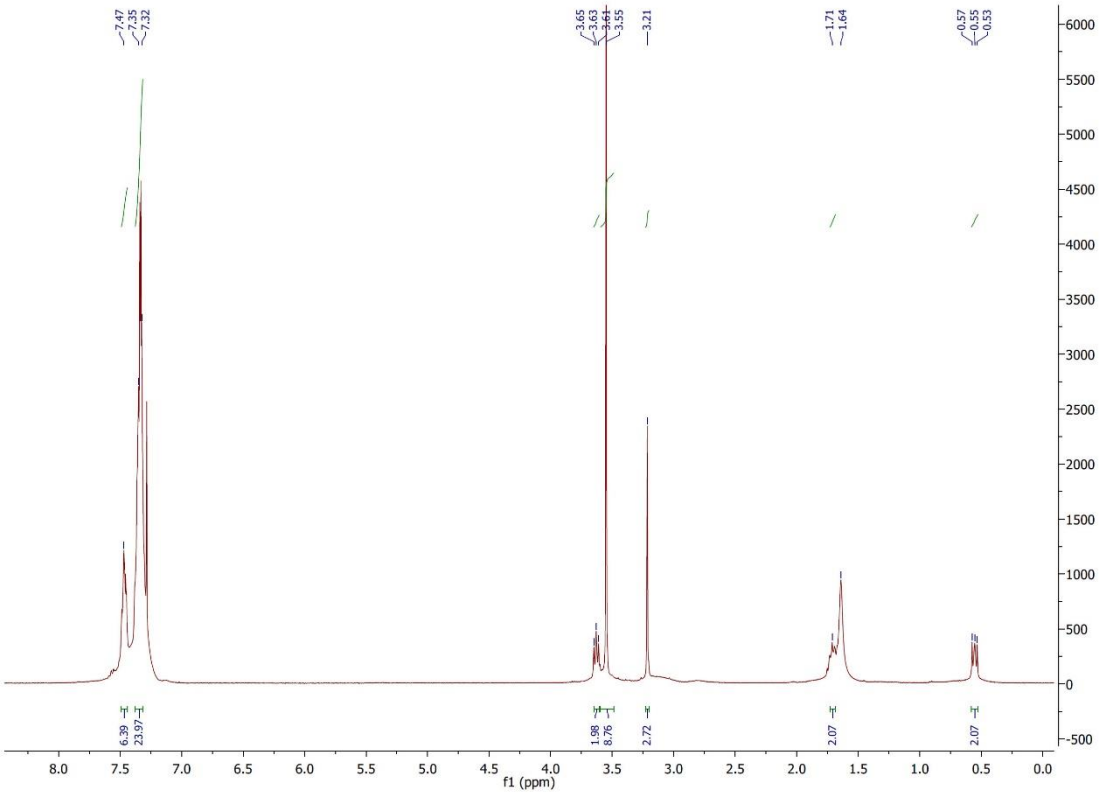

Figure S1-8. ^{1}H NMR spectrum of **3** in $CDCl_3$.

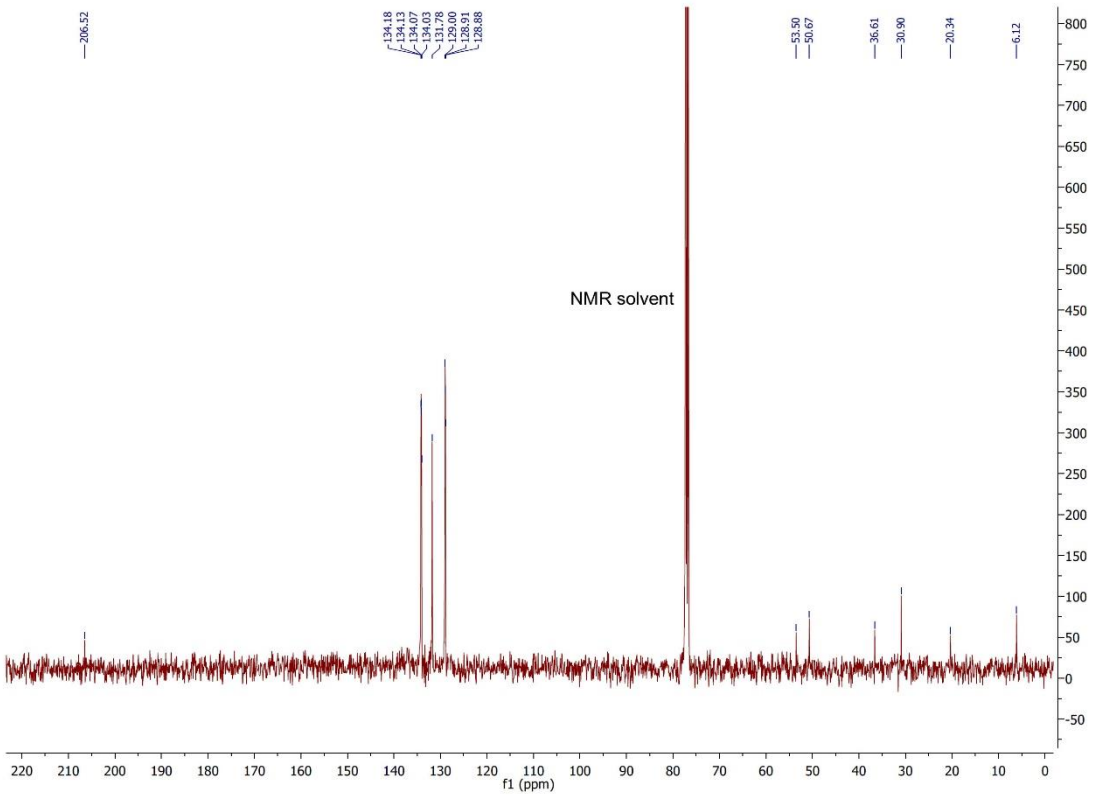

Figure S1-9. $^{13}C\{^{1}H\}$ NMR spectrum of **3** in $CDCl_3$.

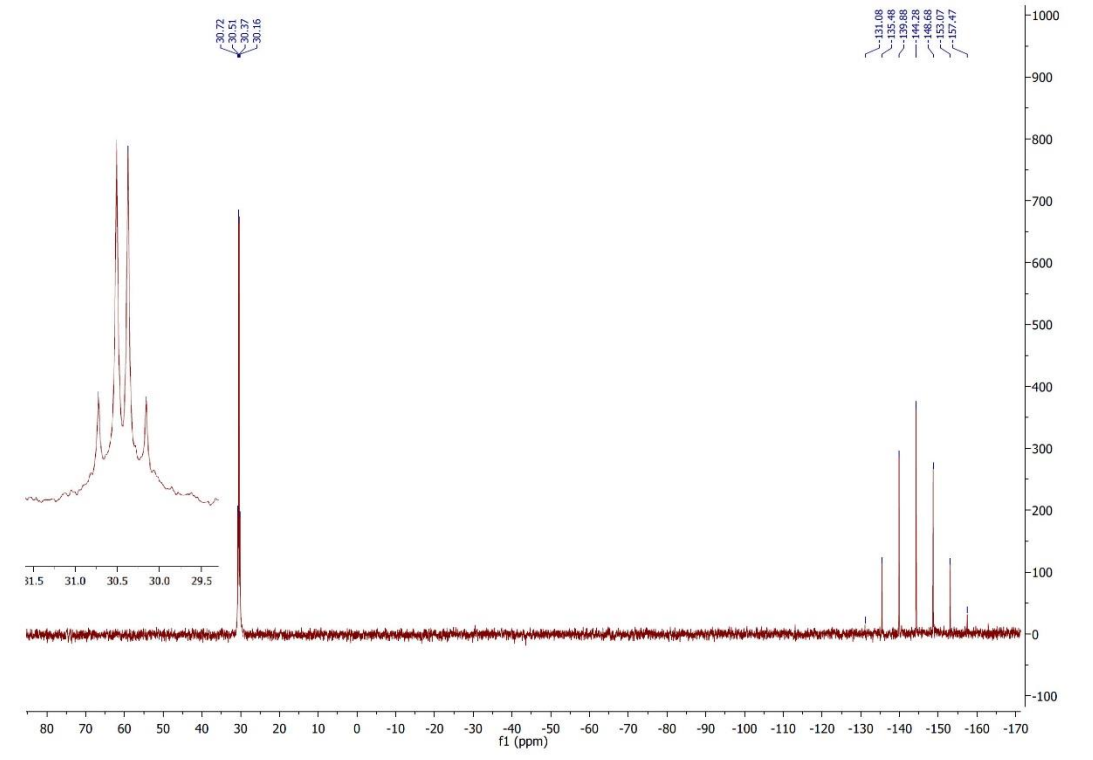

Figure S1-10. $^{31}P\{^{1}H\}$ NMR spectrum of **3** in $CDCl_3$.

[Pd(L2)(PPh$_3$)$_2$]PF$_6$ (4)

a) *cis*-[PdCl$_2$(PPh$_3$)$_2$] (500 mg, 0.71 mmol) was dissolved in CHCl$_3$ (10 mL). K[**L2**] (390 mg, 0.81 mmol) was dissolved in MeOH (10 mL). NH$_4$PF$_6$ (232 mg, 1.42 mmol) was dissolved in MeOH (5 mL). All three solutions were mixed and refluxed under stirring overnight. The solvent was removed and the residue was dissolved in CHCl$_3$ (20 mL). The solution was filtered through Celite and solvent removed. Et$_2$O (20 mL) was added and triturated in an ultrasound bath. The yellow solid product separated by filtration, washed with Et$_2$O (5 mL) and dried under vacuum. Yield: 700 mg (82%). **b)** *trans*-[PdI$_2$(PPh$_3$)$_2$] (20 mg, 0.023 mmol), PPh$_3$ (31.3 mg, 0.138 mmol) and NH$_4$PF$_6$ (6.5 mg, 0.046 mmol) were dissolved in acetonitrile (5 mL). K[**L2**] (11.4 mg, 0.024 mmol) was dissolved in acetonitrile (3 mL) and added dropwise into the mixture. The mixture was left to stir overnight. The solution color changed from orange to yellow. The solvent was removed and the residue was dissolved in CHCl$_3$ (10 mL). The solution was filtered through Celite and solvent removed. Et$_2$O (1 mL) was added and triturated in an ultrasound bath and left in the fridge for the product to precipitate. The product is sparingly soluble in Et$_2$O. The yellow solid product separated by filtration, washed with Et$_2$O (1 mL) and dried under vacuum. Yield: 18.3 mg (68%). IR (ATR): 2941, 2840, 1480 (vCN), 1267 (vC=S), 1188, 1080, 965 (vC-S), 835 (vPF), 744, 692 cm^{-1}. ^{1}H NMR (CDCl$_3$, 400 MHz): δ 0.53 (t, 4H, CH$_2$, J_{HH} = 8.3 Hz), 1.68 (m, 4H, CH$_2$, J_{HH} = 8.3 Hz), 3.52 (s, 18H, OCH$_3$), 3.55 (t, 4H, CH$_2$, J_{HH} = 8.3 Hz), 7.28 - 7.46 (m, 30H, PPh$_3$) ppm. ^{13}C{^{1}H} NMR (CDCl$_3$, 101 MHz): δ 6.3 (s, CH$_2$), 20.7 (s, CH$_2$), 50.7 (s, OCH$_3$), 51.8 (s, CH$_2$), 128.9 (t^v, *o/m*-PC$_6$H$_5$, J_{PC} = 5.3 Hz), 131.8 (s, *p*-PC$_6$H$_5$), 134.1 (*ipso*-PC$_6$H$_5$, obscured), 134.2 (t^v, *o/m*-PC$_6$H$_5$, J_{PC} = 5.8 Hz), 203.1 (s, CS$_2$) ppm. ^{31}P{^{1}H} NMR (CDCl$_3$, 162 MHz): δ -144.3 (sept., PF$_6^-$, J_{PC} = 712.8 Hz), 30.5 (s, PPh$_3$) ppm. MS (ES +ve) *m/z* (abundance): 1047 (88) [M]$^+$. Elem. Anal. Calcd. for C$_{49}$H$_{60}$F$_6$NO$_6$P$_3$PdS$_2$Si$_2$·0.25CHCl$_3$ (M_W = 1192.64, M_W = 1222.48 as solvate): C, 48.4; H, 5.0; N, 1.2%. Found: C, 48.4; H, 5.5; N, 1.6%.

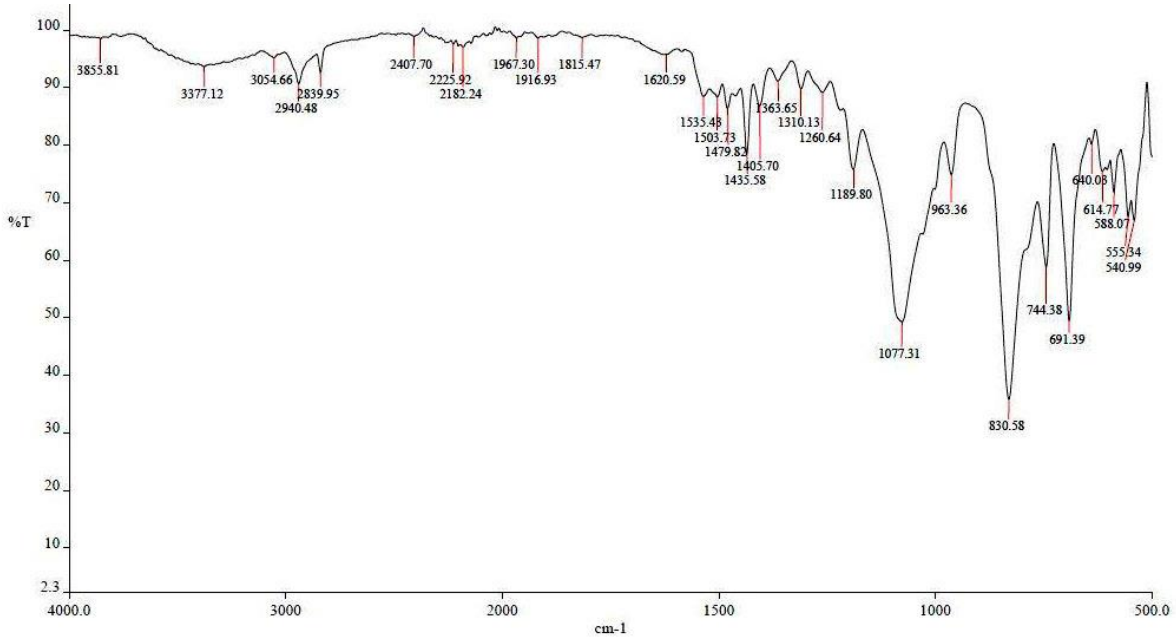

Figure S1-11. Solid state infrared spectrum of **4**.

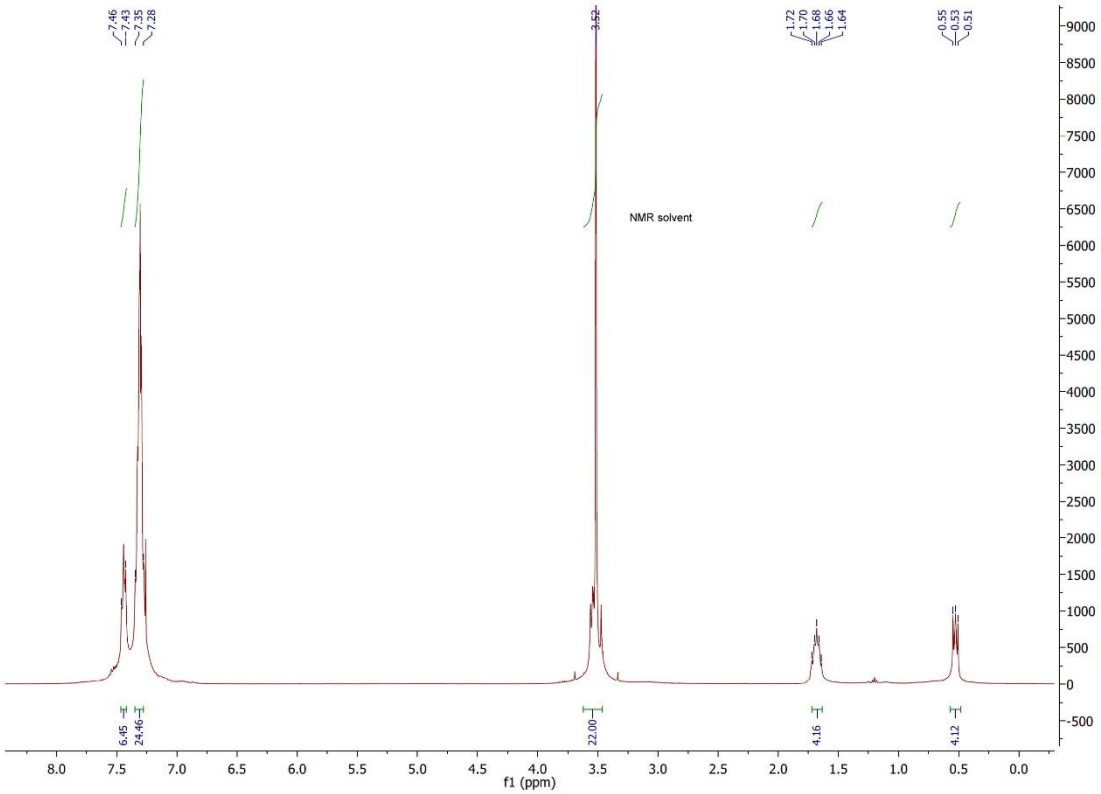

Figure S1-12. ^{1}H NMR spectrum of **4** in $CDCl_3$.

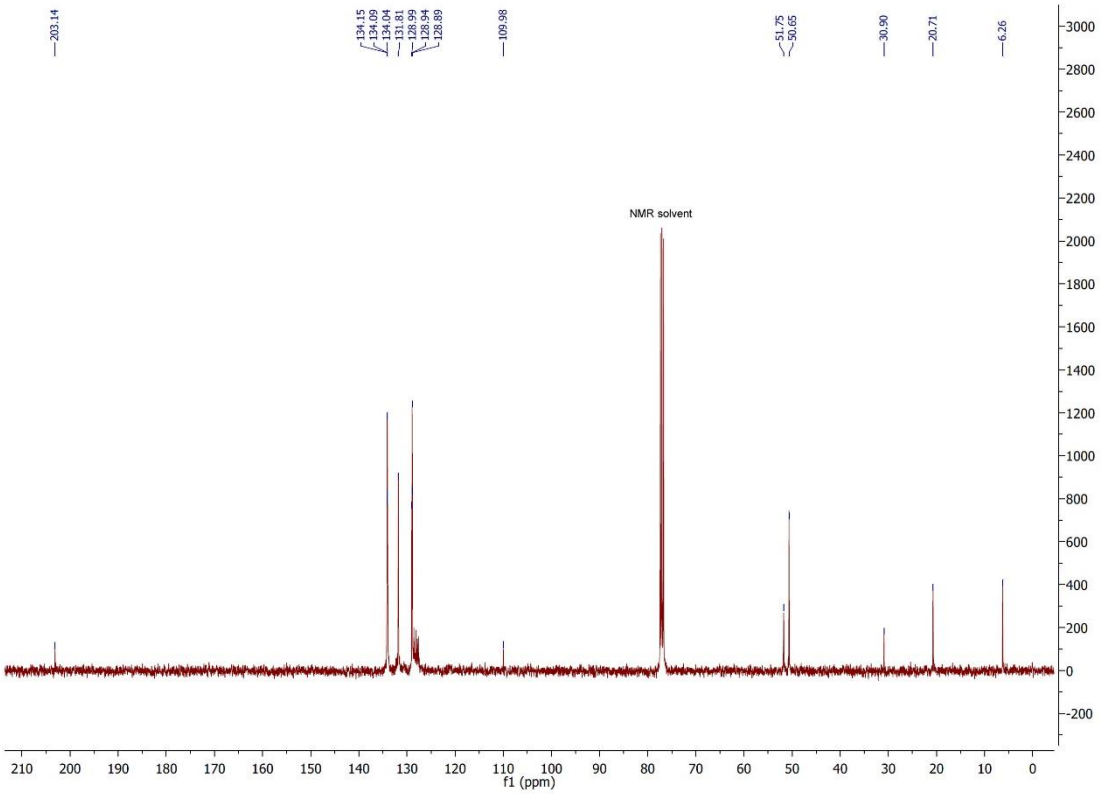

Figure S1-13. $^{13}C\{^{1}H\}$ NMR spectrum of **4** in $CDCl_3$.

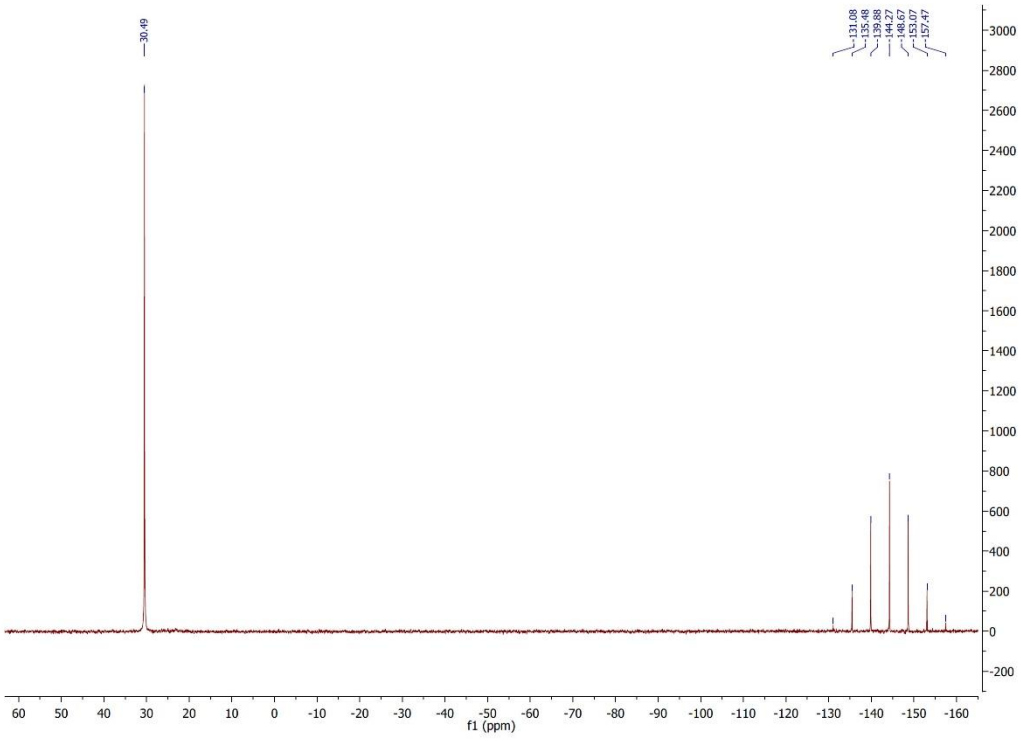

Figure S1-14. $^{31}P\{^{1}H\}$ NMR spectrum of **4** in $CDCl_3$.

[Pd(L1)(dppe)]PF_6 (7)

a) [$PdCl_2$(dppe)] (100 mg, 0.17 mmol) and ammonium hexafluorophosphate (55.4 mg, 0.34 mmol) were dissolved in acetonitrile (10 mL). K[**L1**] (51.4 mg, 0.17 mmol) was dissolved in acetonitrile (5 mL) and added dropwise to the mixture and allowed to stir for 2 hours. The color of the solution changed from white to pale green. The solvent was removed and the residue was dissolved in chloroform (10 mL). The solution was filtered through Celite and solvent removed. Diethyl ether (50 mL) was added and triturated in an ultrasound bath. The green solid product separated by filtration, washed with diethyl ether (5 mL) and dried under vacuum. Yield: 85.6 mg (54%). **b)** [PdI_2(dppe)] (**6**, 30 mg, 0.040 mmol) and NH_4PF_6 (12.9 mg, 0.080 mmol) were dissolved in acetonitrile (5 mL). K[**L1**] (12.1 mg, 0.040 mmol) was dissolved in acetonitrile (5 mL) and added dropwise into mixture and allowed to stir for 2 hours. The color of the solution changed from orange to pale green. The solvent was removed and the residue was dissolved in chloroform (10 mL). The solution was filtered through Celite and solvent removed. Diethyl ether (10 mL) was added and triturated in an ultrasound bath. The green solid product separated by filtration, washed with diethyl ether (5 mL) and dried under vacuum. Yield: 8.0 mg (22%). IR (ATR): 2943, 2364, 2181, 1538, 1484 (vCN), 1435, 1276 (vC=S), 1188, 1077, 964 (vC-S), 832 (vPF), 689 cm^{-1}. ^{1}H NMR ($CDCl_3$, 400 MHz): δ 0.64 (t, 2H, CH_2, J_{HH} = 7.9 Hz), 1.81 (quintet, 2H, CH_2, J_{HH} = 7.9 Hz), 2.83 (d, 4H, PCH_2, J_{HH} = 21.6 Hz), 3.35 (s, 3H, N-CH_3), 3.58 (s, 9H, OCH_3), 3.77 (t, 2H, CH_2, J_{HH} = 7.9 Hz), 7.52 – 7.72 (m, 20H, PPh_3) ppm. $^{13}C\{^1H\}$ NMR ($CDCl_3$, 101 MHz): δ 6.3 (s, CH_2), 20.5 (s, CH_2), 27.0 (t, PCH_2, J_{PC} = 30.2 Hz), 37.0 (s, NCH_3), 50.7 (s, OCH_3), 53.9 (s, CH_2), 129.8 (m, *o/m*-PC_6H_5), 132.6 (s, *p*-PC_6H_5), 132.8 (*ipso*-PC_6H_5, obscured), 132.8 (m, *o/m*-PC_6H_5), 206.4 (s, CS_2) ppm. $^{31}P\{^1H\}$ NMR ($CDCl_3$, 162 MHz): δ -144.3 (sept., PF_6^-, J_{PC} = 711.3 Hz), 59.0 (s, dppe) ppm. MS (ES +ve) *m/z* (abundance): 774 (83) $[M]^+$. Elem. Anal. Calcd. for $C_{34}H_{43}F_6NO_6P_3PdS_2Si$ (M_W = 919.26): C, 44.4; H, 4.7; N, 1.5%. Found: C, 44.3; H, 4.6; N, 1.5%.

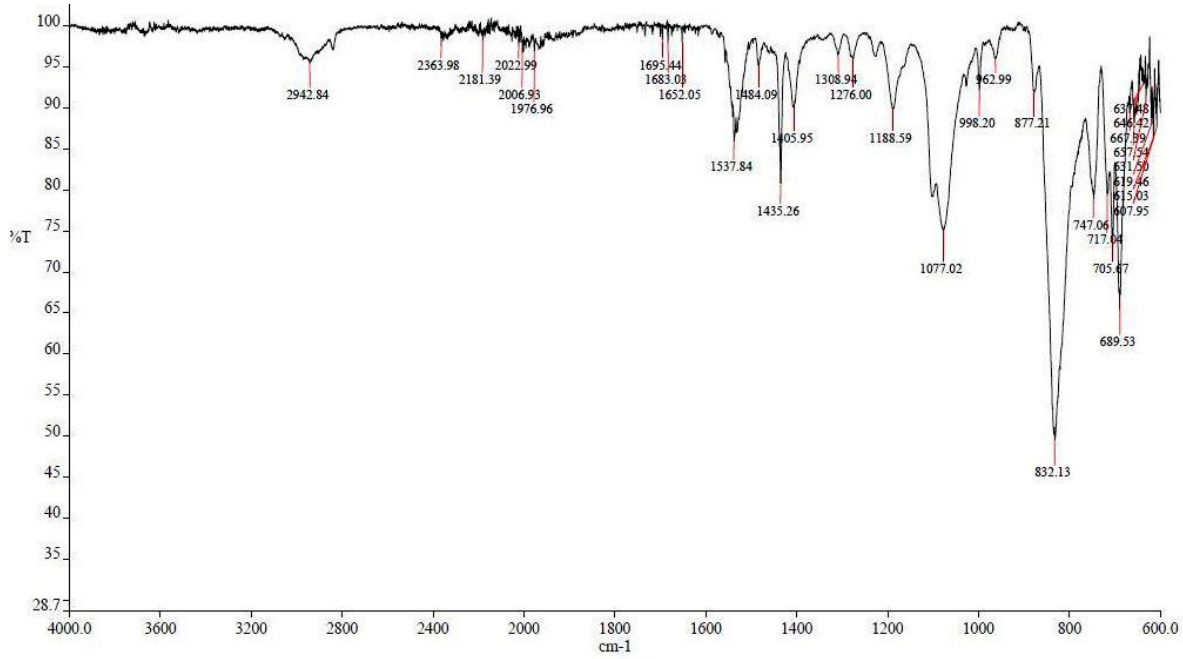

Figure S1-15. Solid state infrared spectrum of **7**.

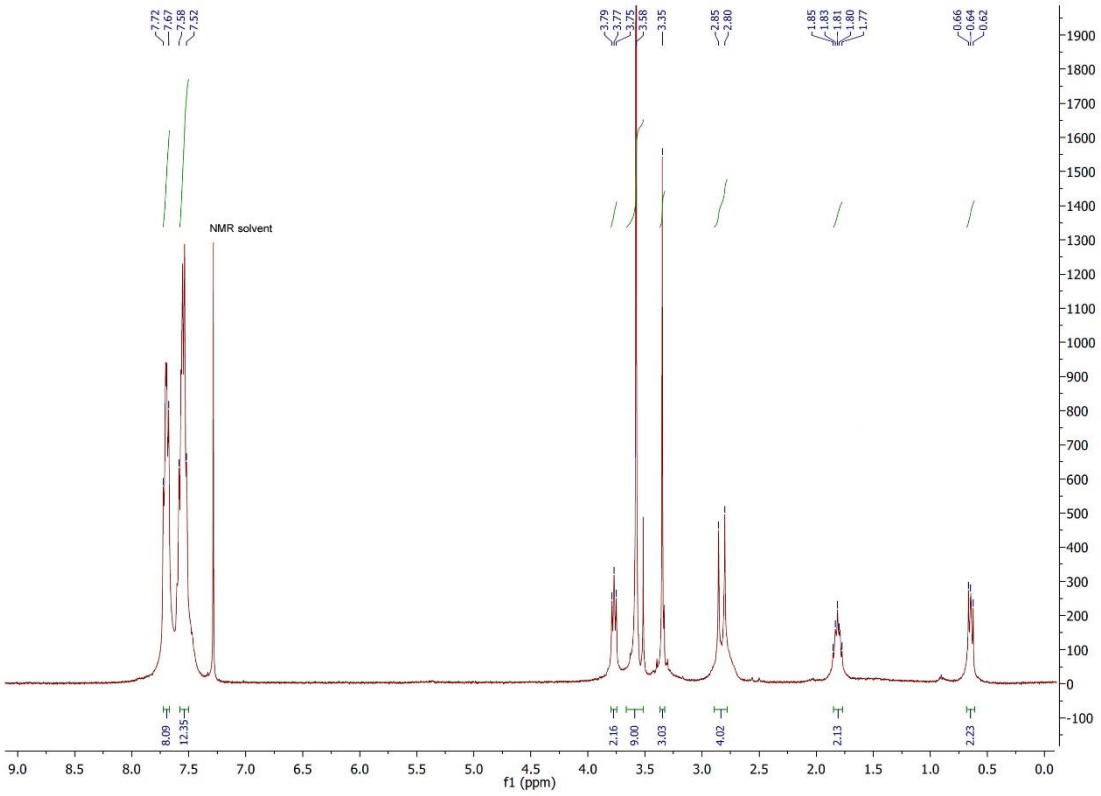

Figure S1-16. ^{1}H NMR spectrum of **7** in $CDCl_3$.

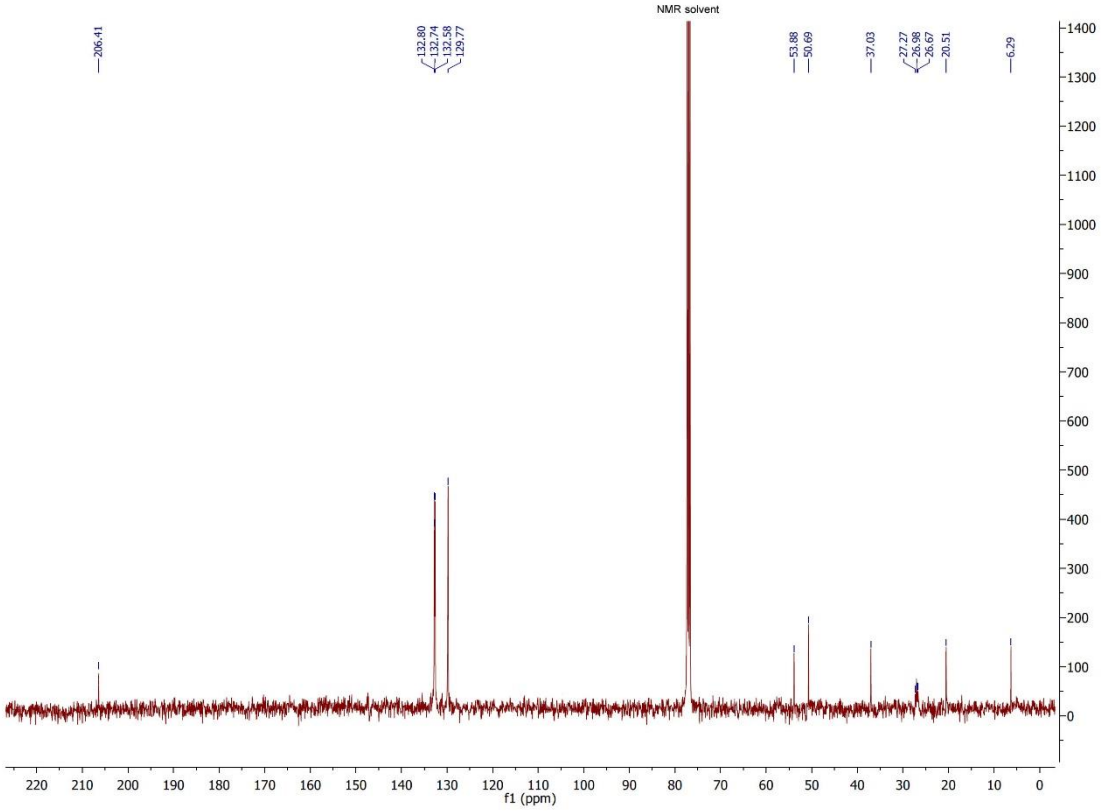

Figure S1-17. $^{13}C\{^{1}H\}$ NMR spectrum of **7** in $CDCl_3$.

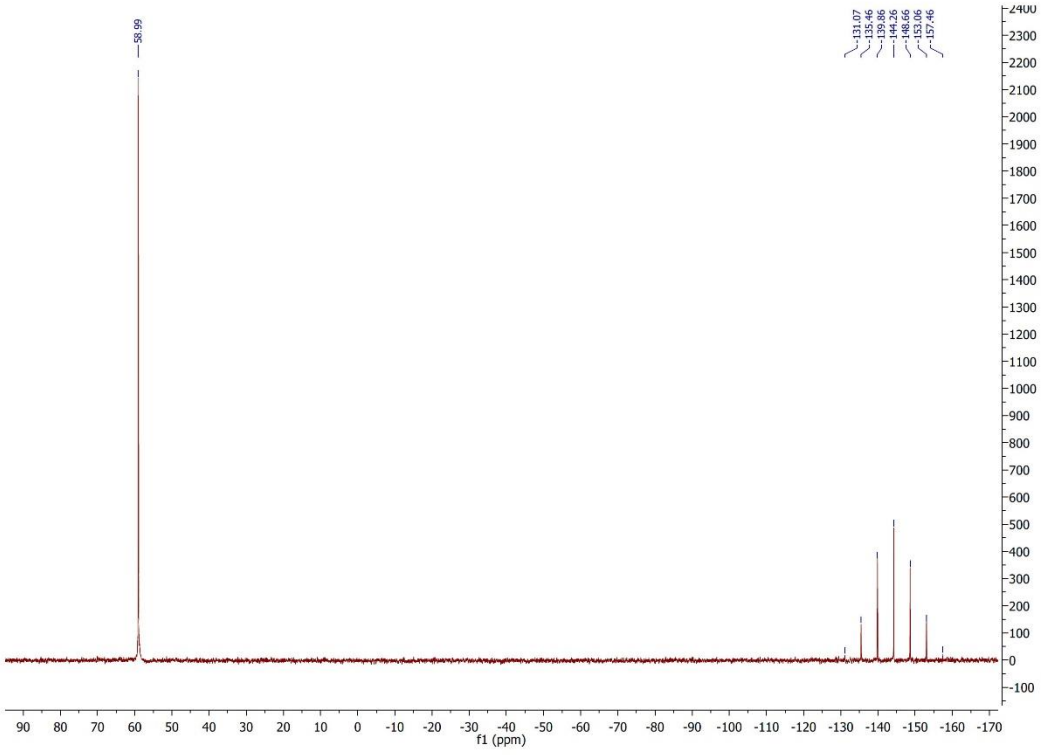

Figure S1-18. $^{31}P\{^{1}H\}$ NMR spectrum of **7** in $CDCl_3$.

[Pd(L2)(dppe)]PF_6 (8)

a) [$PdCl_2$(dppe)] (100 mg, 0.17 mmol) and ammonium hexafluorophosphate (55.4 mg, 0.34 mmol) were dissolved in acetonitrile (10 mL). K[**L2**] (77.7 mg, 0.17 mmol) was dissolved in acetonitrile (5 mL) and added dropwise into mixture and allowed to stir for 2 hours. The color of the solution changed from white to pale green. The solvent was removed and the residue was dissolved in chloroform (10 mL). The solution was filtered through Celite and solvent removed. Diethyl ether (50 mL) was added and triturated in an ultrasound bath. The green solid product separated by filtration, washed with diethyl ether (5 mL) and dried under vacuum. Yield: 88.2 mg (48%). **b)** [PdI_2(dppe)] (**6**, 30 mg, 0.040 mmol) and ammonium hexafluorophosphate (12.9 mg, 0.080 mmol) were dissolved in acetonitrile (5 mL). K[**L2**] (18.3 mg, 0.040 mmol) was dissolved in acetonitrile (5 mL) and added dropwise into mixture and allowed to stir for 2 hours. The color of the solution changed from orange to pale green. The solvent was removed and the residue was dissolved in chloroform (10 mL). The solution was filtered through Celite and solvent removed. Diethyl ether (10 mL) was added and triturated in an ultrasound bath. The green solid product separated by filtration, washed with diethyl ether (5 mL) and dried under vacuum. Yield: 14.6 mg (35%). IR (ATR): 2943, 2839, 2363, 1524, 1484 (vCN), 1435, 1268 (vC=S), 1189, 1077, 998 (vC-S), 878, 834 (vPF), 748, 691 cm^{-1}. ^{1}H NMR ($CDCl_3$, 400 MHz): δ 0.64 (t, 4H, CH_2, J_{HH} = 8.3 Hz), 1.81 (pent., 4H, CH_2, J_{HH} = 8.3 Hz), 2.87 (d, 4H, PCH_2, J_{HH} = 21.9 Hz), 3.57 (s, 18H, OCH_3), 3.71 (t, 4H, CH_2, J_{HH} = 8.3 Hz), 7.52 – 7.73 (m, 20H, C_6H_5) ppm. $^{13}C\{^1H\}$ NMR ($CDCl_3$, 101 MHz): δ 6.4 (s, CH_2), 20.8 (s, CH_2), 27.1 (d, PCH_2, J_{PC} = 23.6 Hz), 50.7 (s, OCH_3), 52.0 (s, CH_2), 129.6 (t^v, *o/m*-PC_6H_5, J_{PC} = 5.6 Hz), 129.7 (s, *p*-PC_6H_5), 134.1 (*ipso*-PC_6H_5, obscured), 132.8 (t^v, *o/m*-PC_6H_5, J_{PC} = 5.7 Hz), 206.9 (s, CS_2) ppm. $^{31}P\{^1H\}$ NMR ($CDCl_3$, 162 MHz): δ -144.3 (sept., J_{PC} = 709.9 Hz), 58.8 (s, dppe) ppm. MS (ES +ve) *m/z* (abundance): 922.1 (88) $[M]^+$. Elem. Anal. Calcd. for $C_{39}H_{55}F_6NO_6P_3PdS_2Si_2 \cdot 2CHCl_3$ (M_W = 1067.49, M_W = 1306.25 for solvate): C, 37.7; H, 4.4; N, 1.1%. Found: C, 37.5; H, 4.2; N, 1.7%.

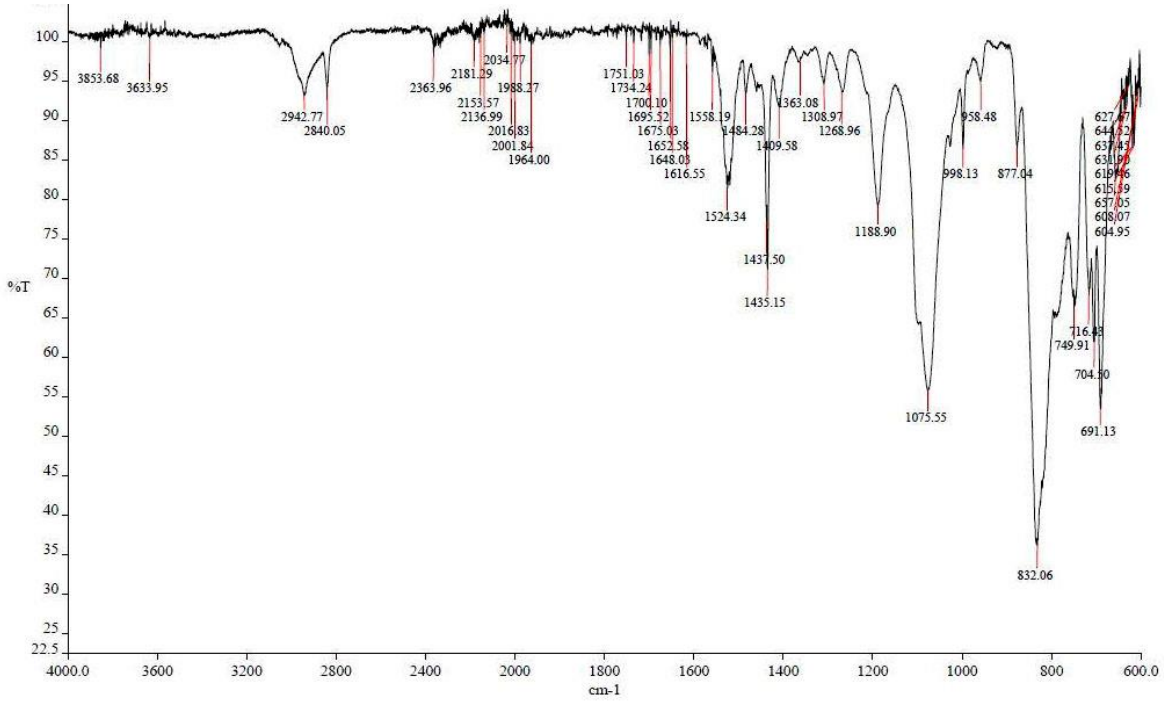

Figure S1-19. Solid state infrared spectrum of **8**.

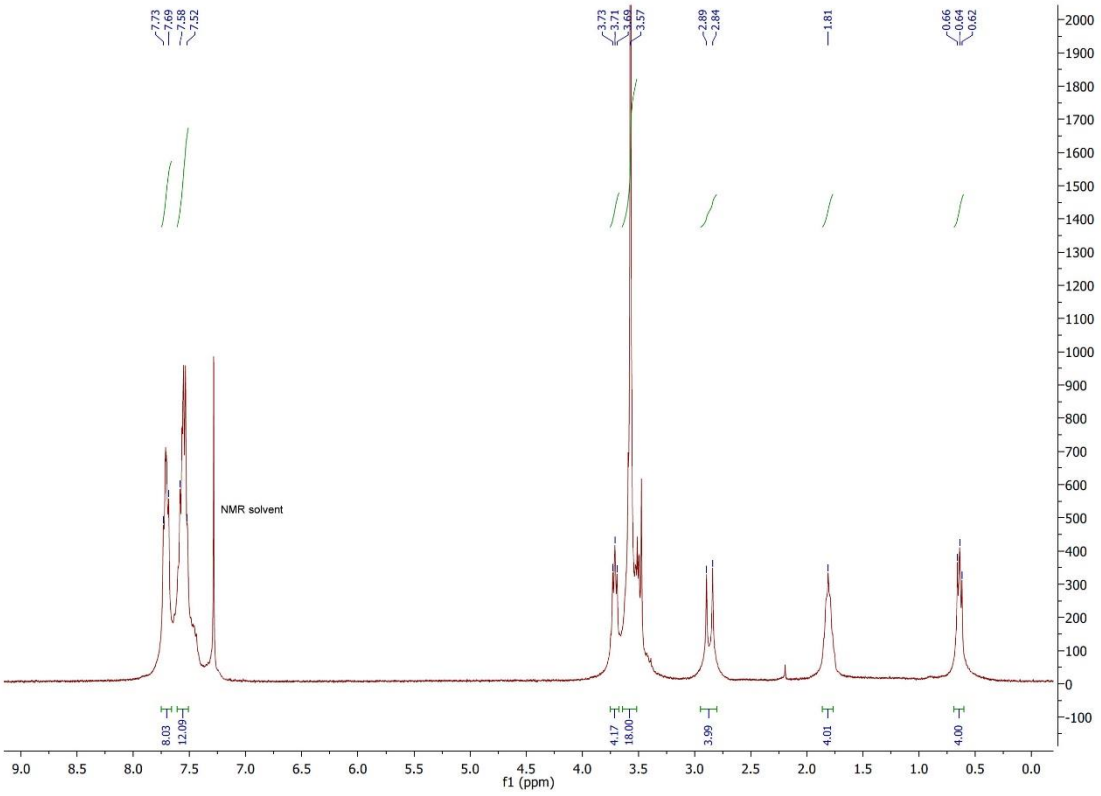

Figure S1-20. ^{1}H NMR spectrum of **8** in $CDCl_3$.

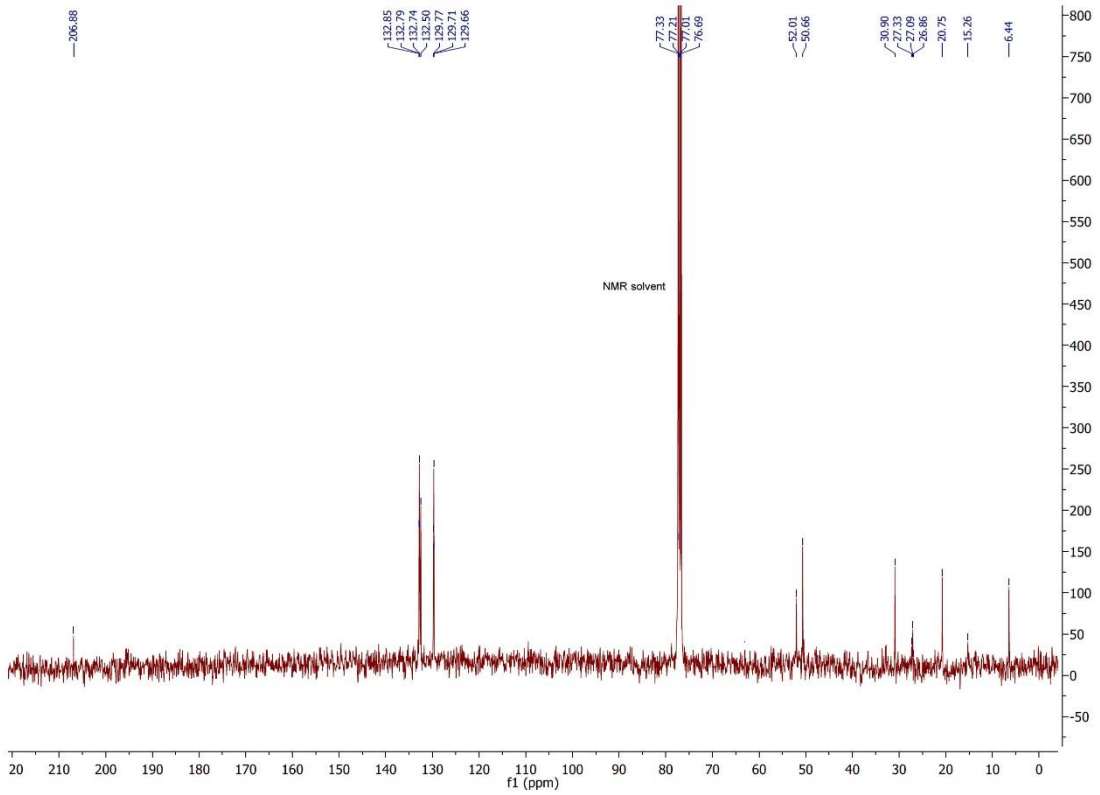

Figure S1-21. $^{13}C\{^{1}H\}$ NMR spectrum of **8** in $CDCl_3$.

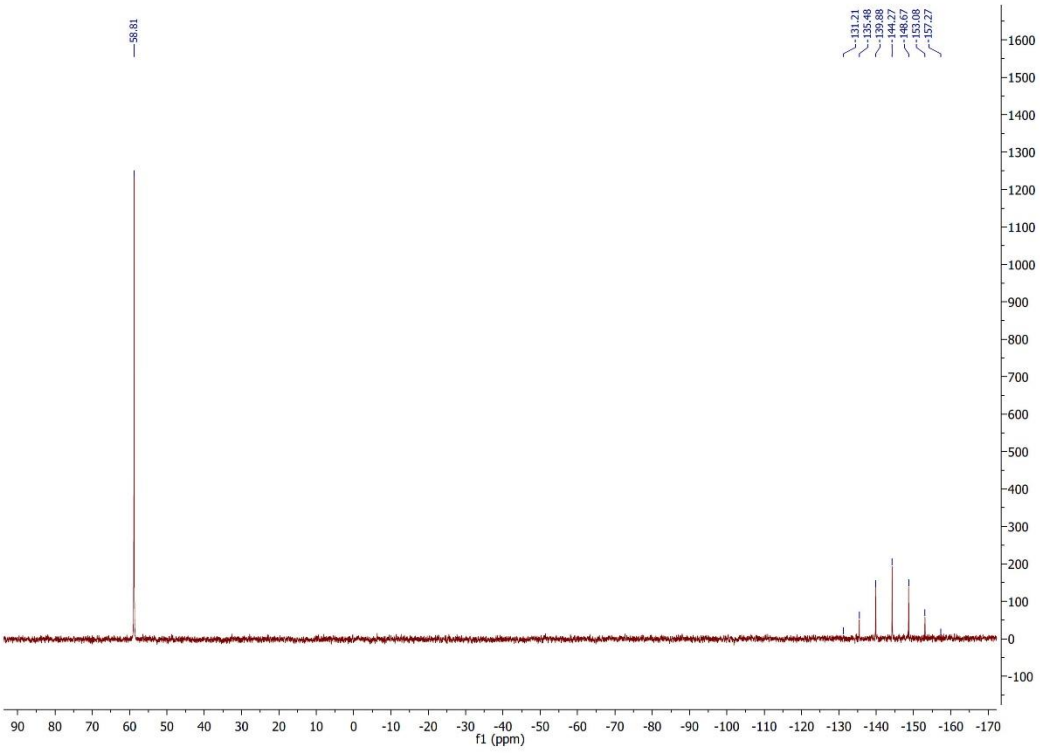

Figure S1-22. $^{31}P\{^{1}H\}$ NMR spectrum of **8** in $CDCl_3$.

Palladium(II) complexes from recovery products

[PdI_2(Me_2dazdt)] (5)

Palladium powder (60 mg, 0.56 mmol), Me_2dazdt (106 mg, 0.56 mmol) and iodine (72 mg, 0.56 mmol) were dissolved in acetone (40 mL) and stirred for 4 hours. A black solution with black precipitate was produced. The black precipitate was separated by filtration and washed with acetone (5 mL) and Et_2O (5 mL), then dried under vacuum. Yield: 269 mg (88%). The remaining acetone solution was placed inside a flask of Et_2O and black crystals of [PdI_2(Me_2dazdt)] were formed by vapor diffusion, allowing a suitable single crystal for X-ray diffraction to be obtained (see Section S2 below). On a smaller scale, a yield of 88% was recorded for 10 mg palladium powder in a shorter reaction time (2h). IR (ATR): 2986, 2925, 1701 (vC-O), 1527, 1395, 1358, 1263, 1114, 958 cm^{-1}. Raman: 1540, 1455, 1404, 1360, 1270, 899, 344, 219, 139, 81 cm^{-1}. ^{1}H NMR (DMSO, 400 MHz): δ 2.41 (t, 2H, CH_2, J_{HH} = 6.8 Hz), 3.59 (s, 6H, CH_3), 3.84 (t, 4H, CH_2, J_{HH} = 6.8 Hz) ppm. MS (ES +ve) *m/z* (abundance): 548 (45) $[M]^+$. Elem. Anal. Calcd. for $C_7H_{12}I_2N_2PdS_2$ (M_W = 548.55): C, 15.3; H, 2.2; N, 5.1%. Found: C, 15.8; H, 2.2; N, 5.5%.

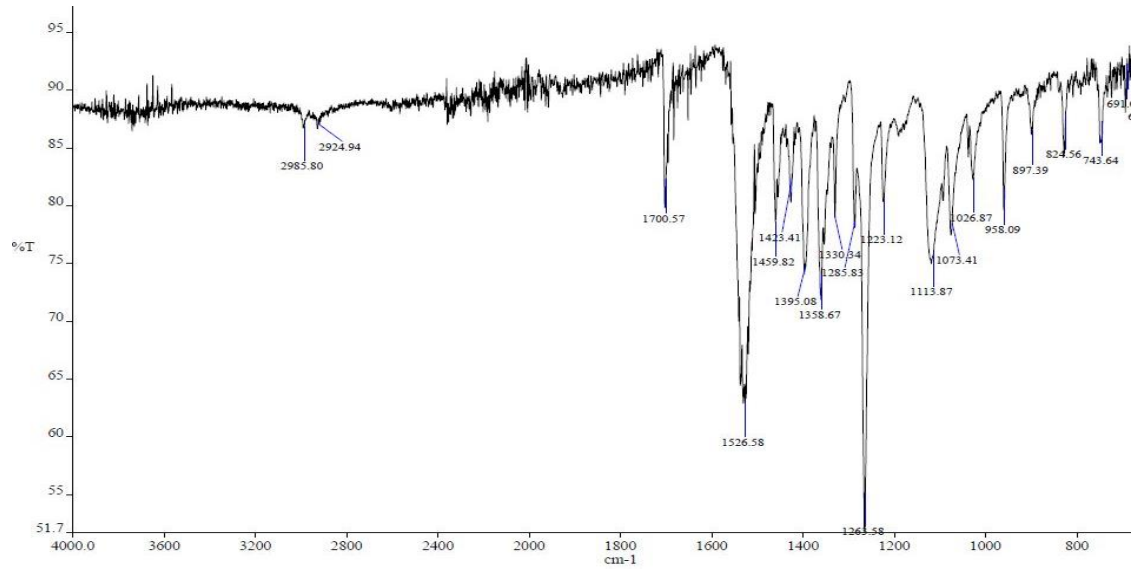

Figure S1-23. Solid state infrared spectrum of **5**.

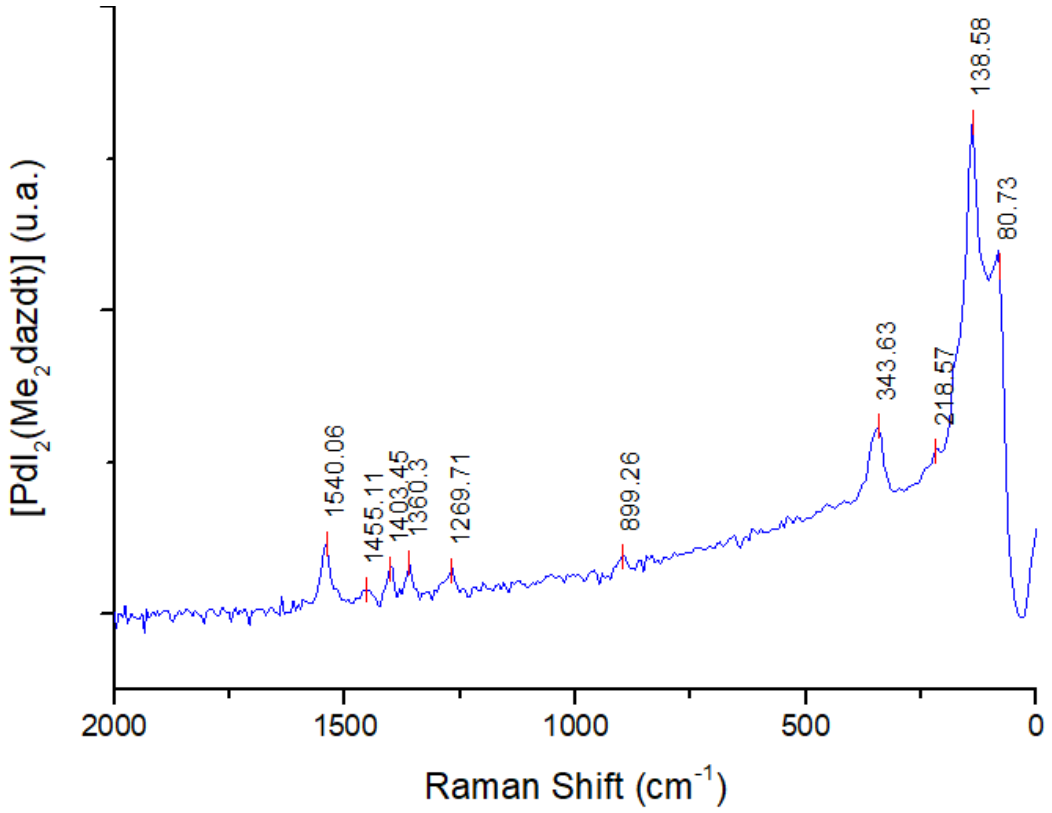

Figure S1-24. Raman spectrum of **5**.

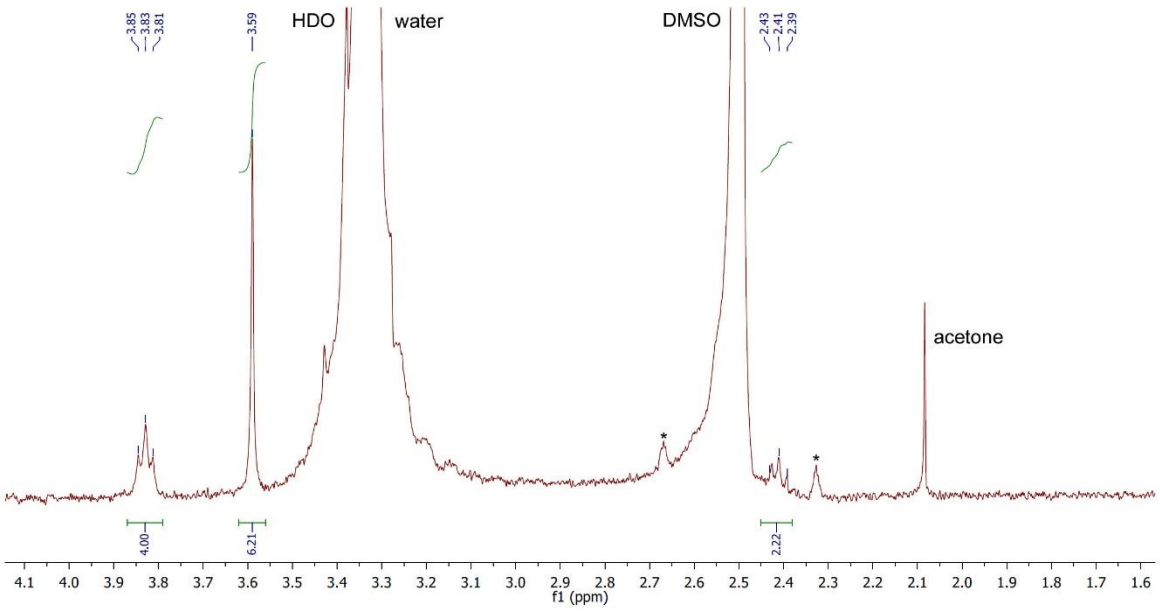

Figure S1-25. ^{1}H NMR spectrum of **5** in d^{6}-DMSO showing the acetone observed in the crystal structure (Figure S3-4). The compound is very insoluble and so the peaks are small compared to those of the residual protons of DMSO and water (HDO also) in the d^{6}-DMSO.

***trans*-[$PdI_2(PPh_3)_2$]**

Compound **5** (60 mg, 0.10 mmol) was dissolved in acetone (10 mL). PPh_3 (51.7 mg, 0.20 mmol, 2 eq) was dissolved in 5 mL of acetone and added dropwise to an acetone solution of **5**. The color of the solution changed from dark brown to orange and an orange precipitate was observed. The solvent was removed and the residue dissolved in $CHCl_3$. Vapor diffusion with Et_2O yielded red crystals, which were separated by filtration and washed with EtOH (5 mL) and Et_2O (5 mL). Yield: 82.7 mg (95%). The following data are in good agreement with those reported previously for this compound.[S4] IR (ATR): 3067, 2973, 1476, 1431, 1092, 997, 746, 689 cm^{-1}. ^1H NMR ($CDCl_3$, 400 MHz): δ 7.64 – 7.75 (m, 30H, PPh_3) ppm. $^{31}P\{^1H\}$ NMR ($CDCl_3$, 162 MHz): δ 12.8 (s, PPh_3) ppm.

[PdI_2(dppe)] (6)

Compound **5** (30 mg, 0.048 mmol) was dissolved in acetone (5 mL). 1,2-bis(diphenylphosphino)ethane (19.7 mg, 0.048 mmol) was dissolved in acetone (5 mL) and added dropwise to an acetone solution of **5**. The color of the solution changed from dark brown to orange and an orange precipitate was observed. The orange precipitate was separated by filtration and washed with ethanol (5 mL) and diethyl ether (5 mL). Yield: 32.5 mg (87%). The following data are in good agreement with those reported previously for this compound.[S5] IR (ATR): 3052, 1437, 1100, 998, 877, 811, 701, 688, 678 cm^{-1}. ^1H NMR ($CDCl_3$, 400 MHz): δ 2.33 (d, 4H, PCH_2, J_{HH} = 23.5 Hz), 7.43 – 7.96 (m, 20H, C_6H_5) ppm. $^{31}P\{^1H\}$ NMR ($CDCl_3$, 162 MHz): δ 61.8 (s, dppe) ppm.

Synthesis of nanoparticles (NPs)

The nanomaterials used in the project (SiO_2,[S6] Fe_3O_4[S7] and $SiO_2@Fe_3O_4$[S8]) were prepared using the Stöber process but following more recent literature procedures.[S6-S9]

Immobilization of complexes 3 and 4 on $SiO_2@Fe_3O_4$ nanoparticles

Under an atmosphere of dry nitrogen, $SiO_2@Fe_3O_4$ nanoparticles (100 mg), compound **3** (100 mg, 0.10 mmol) or **4** (100 mg, 0.08 mmol) were suspended in toluene or chloroform (8 mL). The mixture was refluxed with stirring at 110 °C overnight. The mixture was left to cool and the precipitate was washed with $CHCl_3$ (5 mL). The nanoparticles (**NP1** and **NP2**) were retained with a hand-held magnet and the liquid decanted. The washing process was repeated 10 times and the washing solution collected after each wash analyzed by ^{1}H NMR spectroscopy until no free **3** or **4** was detected. The brown product was dried under vacuum.

3@$SiO_2@Fe_3O_4$ (**NP1**): IR (ATR): 3208, 1063 (ν_{asym}SiO), 944 (ν_{asym}SiOH), 801 (ν_{asym}SiO), 692, 582 (ν_{FeO}) cm^{-1}. EDX data indicated the presence of Si, P, S, Fe and Pd. Further analysis by TGA, TEM and ICP-OES measurements was carried out on the supported catalyst (See Supporting Information section S4).

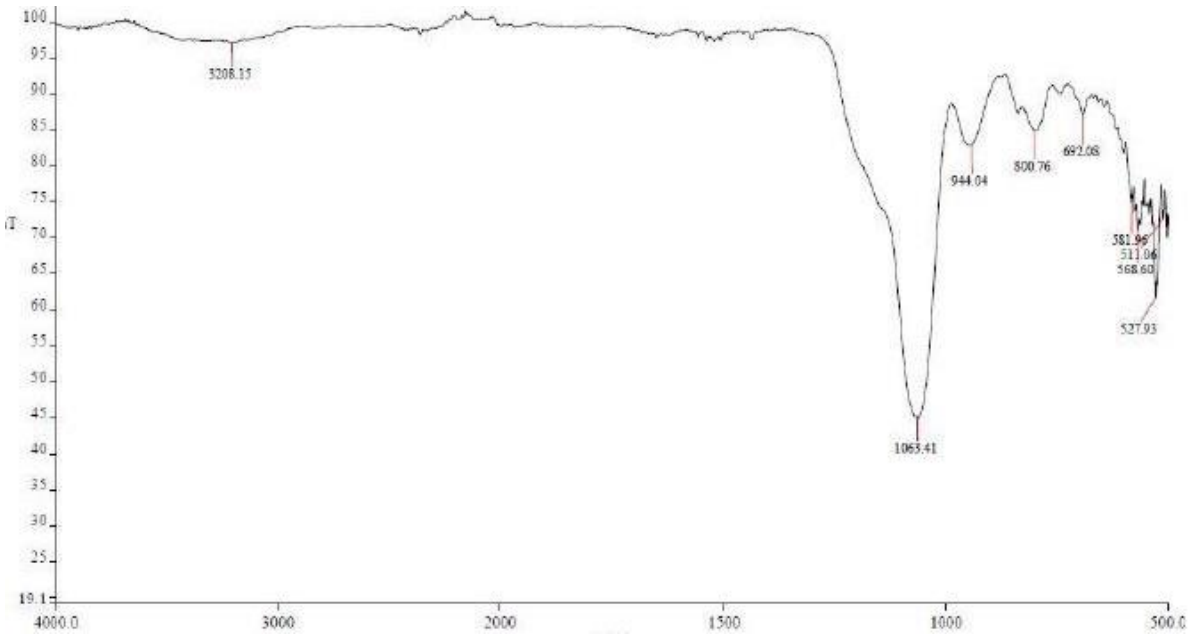

Figure S1-26. Solid state infrared spectrum of **3**@$SiO_2@Fe_3O_4$ (**NP1**).

4@SiO_2@Fe_3O_4 (**NP1**) IR (ATR): 3432, 1059 (ν_{asym}SiO), 947 (ν_{asym}SiOH), 796 (ν_{asym}SiO), 691, 604 (ν_{FeO}) cm^{-1}. EDX data indicated the presence of Si, P, S, Fe and Pd. Further analysis by TGA, TEM and ICP-OES measurements was carried out on the supported catalyst (See Supporting Information section S4).

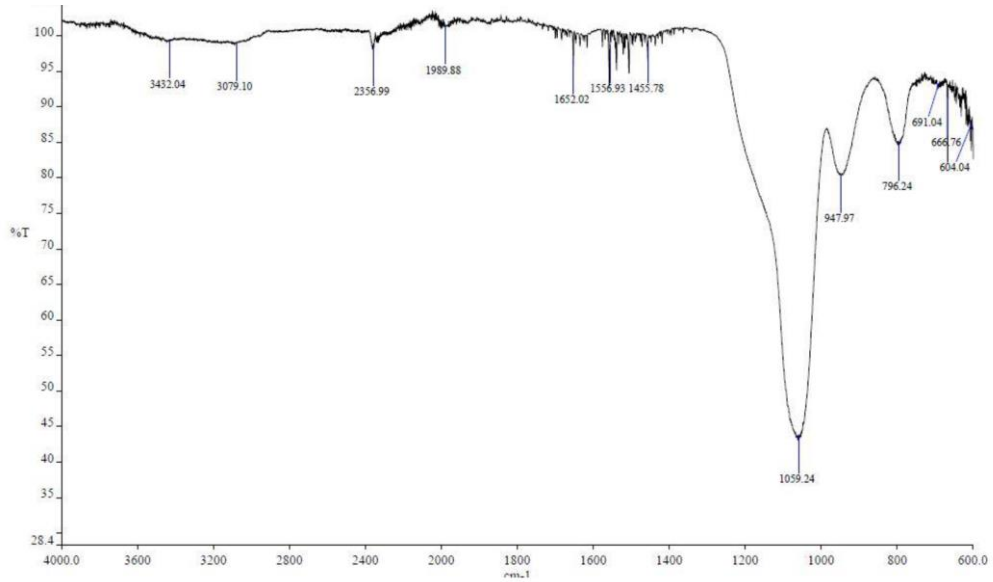

Figure S1-27. Solid state infrared spectrum of **4**@SiO_2@Fe_3O_4 (**NP2**).

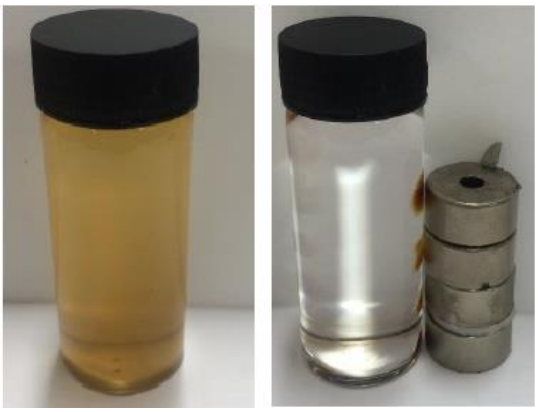

Figure S1-28. Image shows **3**@SiO_2@Fe_3O_4 (**NP1**) being recovered using a hand-held magnet.

S2. Crystallography

The X-ray crystal structure of 3

Crystal data for **3**: $[C_{44}H_{48}NO_3P_2PdS_2Si](PF_6)\cdot 0.5(CH_2Cl_2)$, M = 1086.81, monoclinic, *I*2/*a* (no. 15), a = 20.7257(5), b = 19.2506(5), c = 49.4978(9) Å, β = 97.0520(16)°, V = 19599.3(8) Å^3, Z = 16 [two independent molecules], D_c = 1.473 g cm^{-3}, μ(Mo-Kα) = 0.703 mm^{-1}, T = 173 K, yellow blocks, Agilent Xcalibur 3 E diffractometer; 19677 independent measured reflections (R_{int} = 0.0247), F^2 refinement,[S10,S11] R_1(obs) = 0.0461, wR_2(all) = 0.0955, 14109 independent observed absorption-corrected reflections [$|F_o| > 4\sigma(|F_o|)$, completeness to θ_{full}(25.2°) = 98.8%], 1263 parameters. CCDC 1882025.

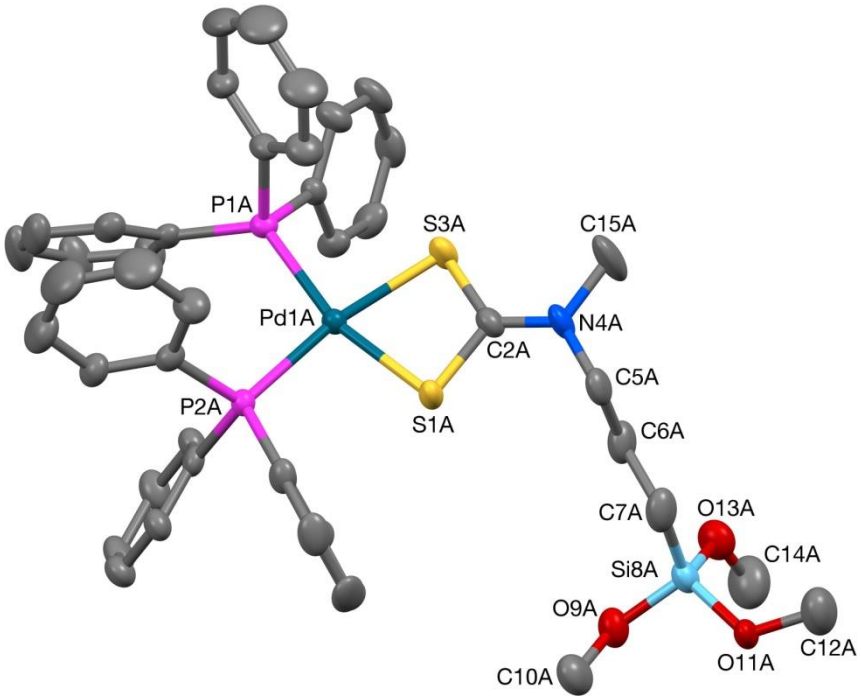

Figure S2-1. The structure of one (**3-A**) of the two independent cationic complexes present in the crystal of **3** (50% probability ellipsoids).

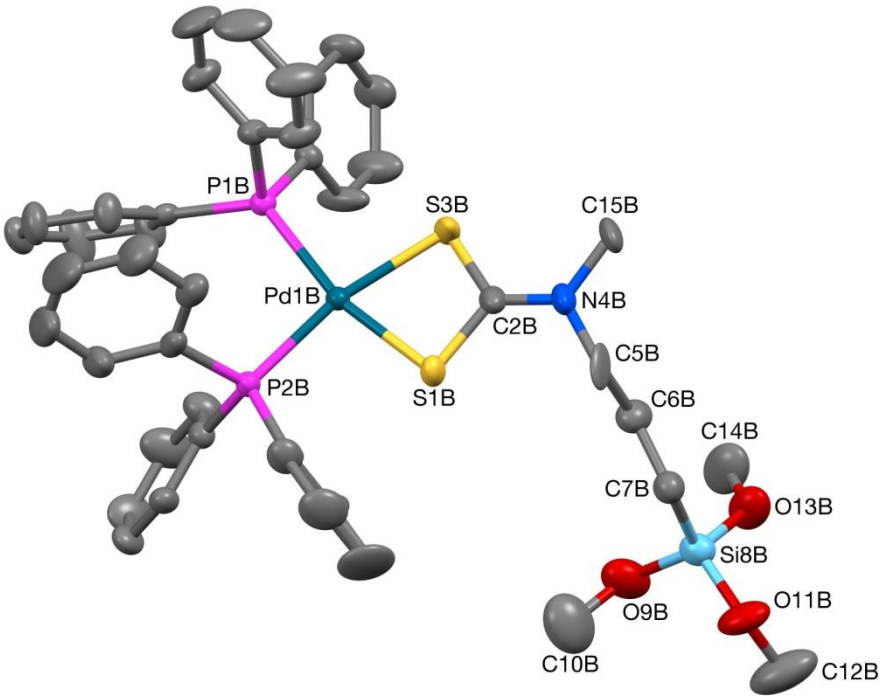

Figure S2-2. The structure of one (**3-B**) of the two independent cationic complexes present in the crystal of **3** (50% probability ellipsoids).

The structure of **3** was found to contain two crystallographically independent molecules (**3-A** and **3-B**) in the asymmetric unit, and significant disorder was found in both molecules. For molecule **3-A**, two orientations were identified for the –$Si(OMe)_3$ unit, and the C22A-, C40A-, and C46A-based phenyl rings, of *ca*. 58:42, 71:29, 58:42, and 72:28% occupancy respectively. For molecule **3-B**, two orientations were identified for the –N(Me)–$(CH_2)_3$–$Si(OMe)_3$ moiety (with a common nitrogen position), and the C28B-, C40B-, and C46B-based phenyl rings, of *ca*. 53:47, 59:41, 60:40, and 55:45% occupancy respectively. The P60-based PF_6 anion was also found to be disordered, and two orientations were identified of *ca*. 75 and 25% occupancy. In all nine instances the geometries of the two orientations were optimized, the thermal parameters of adjacent atoms were restrained to be similar, and only the non-hydrogen atoms of the major occupancy orientations were refined anisotropically (those of the minor occupancy orientations were refined isotropically). The included dichloromethane solvent was found to occupy two sites in the asymmetric unit, both of which are close to a C_2 axis. In each case this was modelled using one unique, 50% occupancy, orientation (with a second 50% occupancy orientation being generated by operation of the C_2 axis) without any restraints, and all of the non-hydrogen atoms were refined anisotropically.

The X-ray crystal structure of 4

Crystal data for **4**: $[C_{49}H_{60}NO_6P_2PdS_2Si_2](PF_6)$, M = 1192.59, triclinic, P-1 (no. 2), a = 12.9734(6), b = 14.7655(6), c = 16.2359(7) Å, α = 63.882(4), β = 76.579(4), γ = 81.131(3)°, V = 2711.5(2) Å^3, Z = 2, D_c = 1.461 g cm^{-3}, μ(Cu-Kα) = 5.322 mm^{-1}, T = 173 K, pale yellow plates, Agilent Xcalibur PX Ultra A diffractometer; 10370 independent measured reflections (R_{int} = 0.0339), F^2 refinement,[S10,S11] R_1(obs) = 0.0423, wR_2(all) = 0.1163, 8644 independent observed absorption-corrected reflections [$|F_o| > 4\sigma(|F_o|)$, completeness to θ_{full}(67.7°) = 98.2%], 682 parameters. CCDC 1882026.

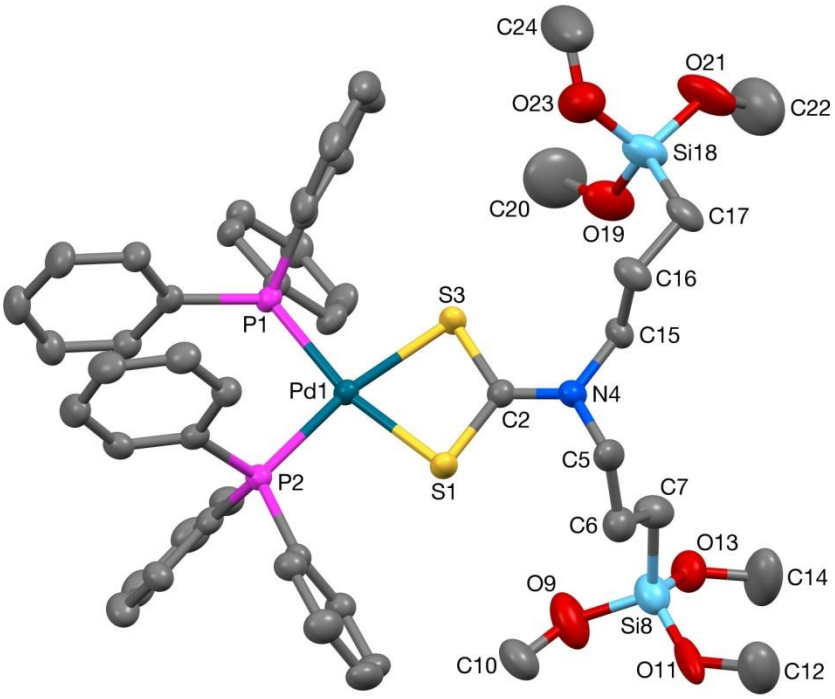

Figure S2-3. The crystal structure of the cationic complex **4** (50% probability ellipsoids).

Both of the $Si(OMe)_3$ units in the structure of **4** were found to be disordered. In each case two orientations were identified (with common silicon positions) of *ca*. 73:27 and 83:17% occupancy for the Si8- and Si18-based units respectively. The geometries of each pair of orientations were optimized, the thermal parameters of adjacent atoms were restrained to be similar, and only the non-hydrogen atoms of the major occupancy orientations were refined anisotropically (those of the minor occupancy orientations were refined isotropically).

The X-ray crystal structure of 5

Table S2-1. Crystal data and structure refinement for **5**·acetone

Empirical formula	$C_{10}H_{18}N_2S_2PdI_2O$
Formula weight	606.58
Temperature/K	296.15
Crystal system	monoclinic
Space group	C2/c
a/Å	7.3789(7)
b/Å	18.960(2)
c/Å	12.759(1)
α/°	90
β/°	103.319(1)
γ/°	90
Volume/Å^3	1737.1(3)
Z	4
ρ_{calc}g/cm^3	2.319
μ/mm^{-1}	4.855
F(000)	1136.0
Crystal size/mm^3	0.32 × 0.24 × 0.17
Radiation	MoKα (λ = 0.71073)
2θ range for data collection/°	2.148 to 30.596
Index ranges	-10 ≤ h ≤ 10, -26 ≤ k ≤ 27, -18 ≤ l ≤ 18
Reflections collected	12607
Independent reflections	2682 [R_{int} = 0.0379]
Data/restraints/parameters	2682/0/86
Goodness-of-fit on F^2	1.054
Final R indexes [I>=2σ (I)]	R_1 = 0.0260, wR_2 = 0.0558
Largest diff. peak/hole / e Å^{-3}	0.96/-0.47

$R1 = \Sigma||F_O|-|F_C||/\Sigma|F_O|$, $wR2 = [\Sigma[w(F_O^2-F_C^2)^2]/\Sigma[w(F_O^2)^2]]^{½}$, $w = 1/[\sigma^2(F_O^2) + (aP)^2 + bP]$, where $P = [\max(F_O^2,0) + 2F_C^2]/3$

Single crystal data for the black blocky crystals were collected with a Bruker Smart Breeze area detector diffractometer (Mo Kα: λ = 0.71073 Å). The intensity data were integrated from several series of exposures frames (0.3° width) covering the sphere of reciprocal space (SMART (control) and SAINT (integration) software for CCD systems; Bruker AXS: Madison, WI, 1994). Absorption corrections were applied using the program SADABS (Siemens Industrial Automation, Inc.: Madison, WI, 1996). The structure was solved by the dual space algorithm implemented in the SHELXT code[S12] and refined on F^2 with full-matrix least squares (SHELXL-2014),[S13] using the Olex2 package.[S14] Non-hydrogen atoms were refined anisotropically, and the hydrogen atoms were placed at their calculated positions. CCDC 1882027.

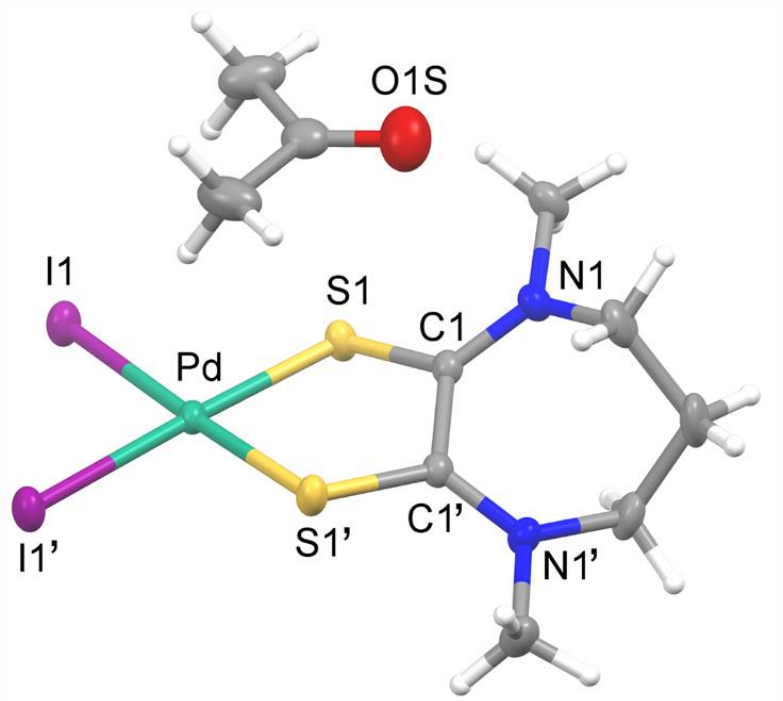

Figure S2-4. Molecular structure of **5**·acetone with thermal ellipsoids drawn at the 30% probability level. Symmetry = 1-x; y; 1/2-z.

In the molecular structure of **5**·acetone, the metal displays a square planar geometry. The asymmetric unit comprises half of the molecular entity since the molecule lies on a two-fold axis. The complex and the molecule of acetone of crystallization form a stacking motif, which is parallel to the *a* crystallographic axis, as shown in Figure S3-5. Adjacent stacks interact weakly with each other through the iodide anions and the methyl and methylene groups of the sulfur chelate.

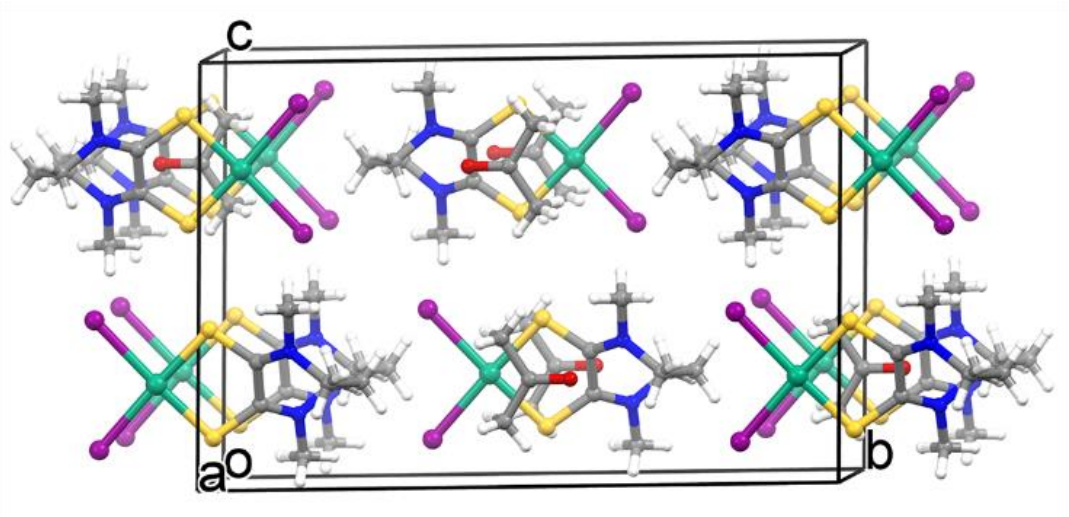

Figure S2-5. Crystal packing of **5**·acetone projected along the crystallographic axis.

The X-ray crystal structure of 7

Crystal data for **7**: $[C_{34}H_{42}NO_3P_2PdS_2Si](PF_6)$, M = 918.20, triclinic, P-1 (no. 2), a = 9.9968(6), b = 13.1257(7), c = 16.8401(9) Å, α = 71.730(5), β = 74.187(5), γ = 85.809(5)°, V = 2018.7(2) $Å^3$, Z = 2, D_c = 1.511 g cm^{-3}, μ(Cu-Kα) = 6.629 mm^{-1}, T = 173 K, colorless plates, Agilent Xcalibur PX Ultra A diffractometer; 7683 independent measured reflections (R_{int} = 0.0444), F^2 refinement,[S10,S11] R_1(obs) = 0.0600, wR_2(all) = 0.1828, 5842 independent observed absorption-corrected reflections [$|F_o| > 4\sigma(|F_o|)$, completeness to θ_{full}(67.7°) = 98.1%], 521 parameters. CCDC 1882028.

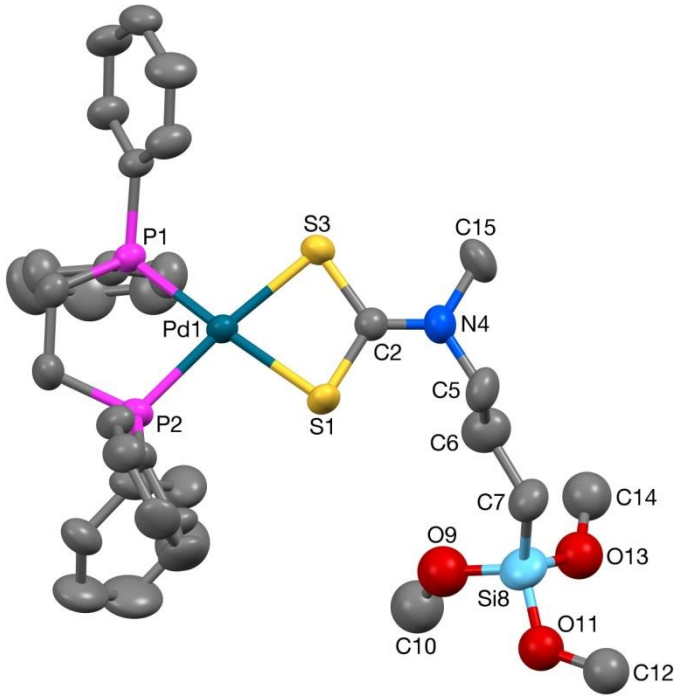

Figure S2-6. The crystal structure of the cationic complex **7** (50% probability ellipsoids).

The $Si(OMe)_3$ unit in the structure of **7** was found to be severely disordered. Three orientations were identified of *ca*. 46, 28 and 26% occupancy, their geometries were optimized, the thermal parameters of adjacent atoms were restrained to be similar, and only the silicon atom of the major occupancy orientation was refined anisotropically (all of the other atoms were refined isotropically). The C30- and C36-based phenyl rings, and the PF_6 anion, were also found to be disordered and in each case two orientations were identified, of *ca*. 73:27, 63:37, and 86:14% occupancy

respectively. The geometries of each pair of orientations were optimized, the thermal parameters of adjacent atoms were restrained to be similar, and only the non-hydrogen atoms of the major occupancy orientations were refined anisotropically (those of the minor occupancy orientations were refined isotropically).

S3. TEM, TGA and ICP-OES data

Transmission Electron Microscopy: TEM investigations were performed on a JEOL 2010 high-resolution TEM (80−200 kV) equipped with an Oxford Instruments INCA EDS 80 mm X-Max detector system, using holey carbon film on 3.05 mm diameter 300 mesh copper grid. Samples were prepared by adding a small drop of the nanoparticle solution suspended in methanol to the grid and allowing the liquid to dry in air at room temperature.

The sizes of the nanoparticles were obtained by manually measuring 60 randomly chosen particles on the TEM image and by averaging the results.

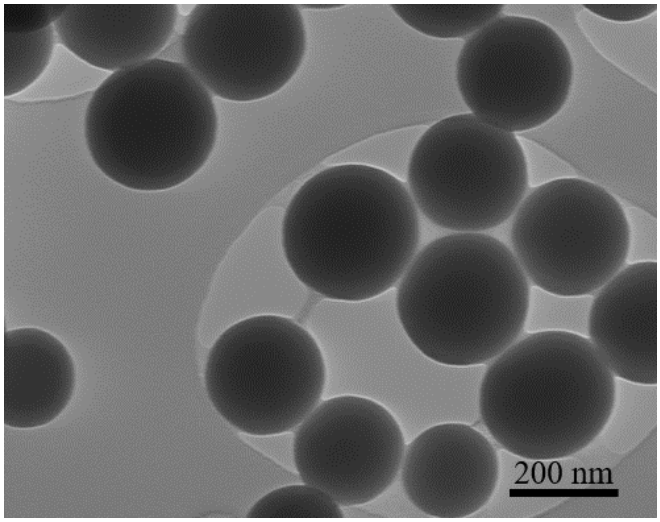

Figure S3-1. TEM images of the silica nanoparticles synthesized (201 ± 40 nm).

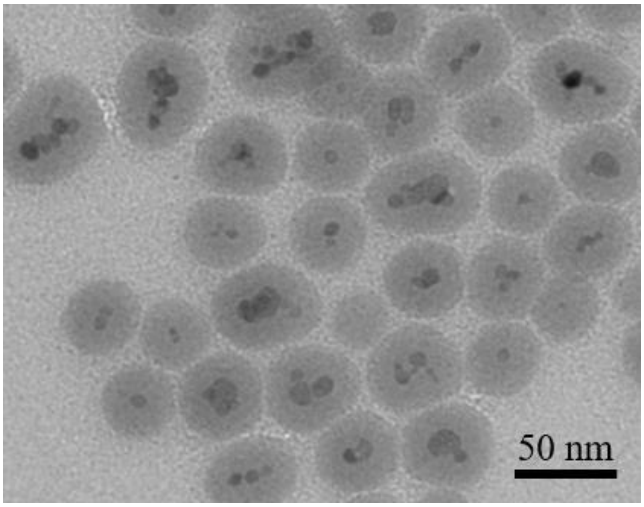

Figure S3-2. TEM images of the SiO_2@Fe_3O_4 core-shell nanoparticles synthesized (41.0 ± 4.3 nm).

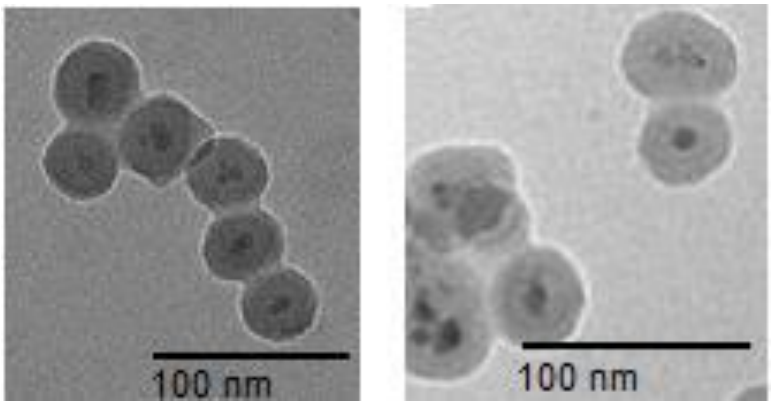

Figure S3-3. TEM images of immobilized palladium complexes **3**@SiO_2@Fe_3O_4 (**NP1**) on the left (40.7 ± 3.2 nm) and **4**@SiO_2@Fe_3O_4 (**NP2**) on the right (43.2 ± 3.3 nm).

Thermogravimetric Analysis: TGA studies were performed on dried nanoparticle samples using a Mettler Toledo TGA with a quasi-isothermal heating (30-100°C hold for 20 min and then 100-600°C with 10 °C per minute increases). The values were reported as a relative percentage of the mass lost compared to the mass at 100 °C.

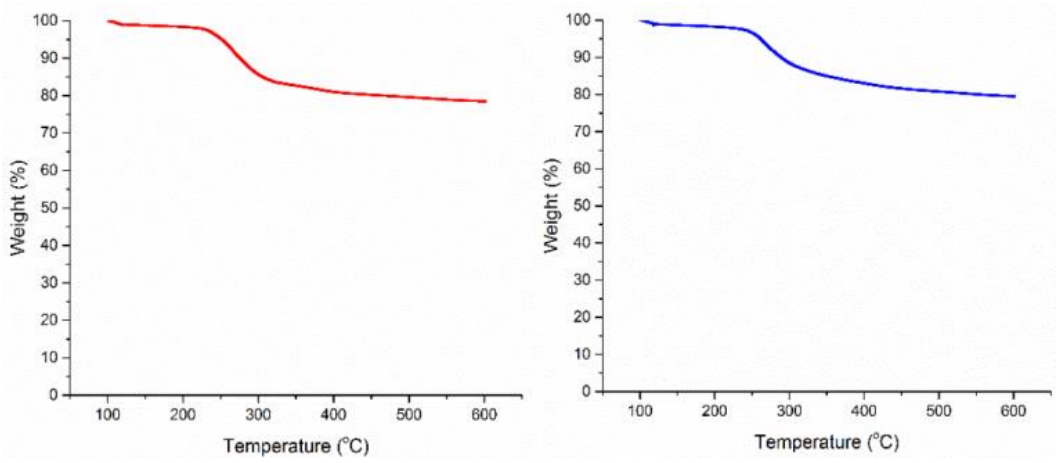

Figure S3-4. TGA data for the immobilized palladium complexes **3**@SiO_2@Fe_3O_4 (**NP1**) on the left and **4**@SiO_2@Fe_3O_4 (**NP2**) on the right.

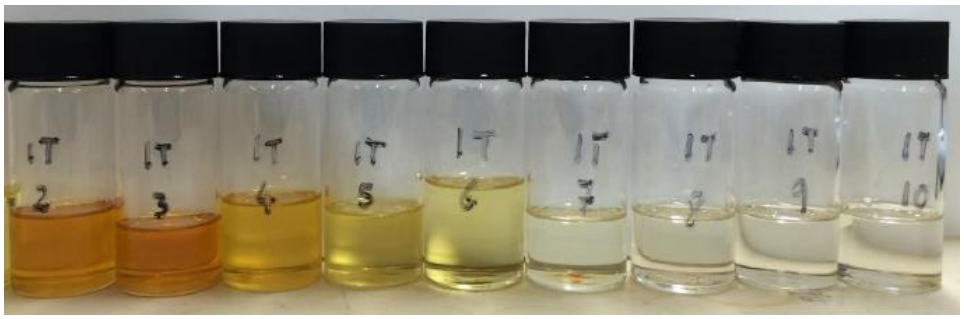

Figure S3-5. Washings to remove unattached surface units from **3**@SiO_2@Fe_3O_4 (**NP1**).

Inductively-Coupled Plasma Optical Emission Spectrometry: The palladium content in **3**@SiO_2@Fe_3O_4 (**NP1**) and **4**@SiO_2@Fe_3O_4 (**NP1**) was determined using ICP-OES. Approximately 1 mg of sample was dissolved in a solution of *aqua regia* (3 mL HCl / 1 mL HNO_3) and the mixture was then stirred and heated at 100 °C for 2 hours and then diluted with de-ionized water to decrease the concentration of acid to less than 10% (v/v). According to the analysis, in the materials prepared in refluxing toluene, the palladium unit contributed 9.0% and 10.0% of the total mass of **3**@SiO_2@Fe_3O_4 (**NP1**) and **37**@SiO_2@Fe_3O_4 (**NP2**), respectively (Table S3-1). When

chloroform was used to heat the reaction, a lower Pd loading was obtained. A significant loss in surface units was found when performing the analysis after catalysis.

Table S3-1. ICP-OES data for the immobilized palladium complexes **3**@SiO_2@Fe_3O_4 (**NP1**) and **4**@SiO_2@Fe_3O_4 (**NP2**).

Sample	Loading (w.r.t total mass)	Loading (w.r.t total Silica)	Conditions
NP1	9.0%	9.9%	Reflux in toluene, overnight
NP2	10.0%	11.1%	Reflux in toluene, overnight
NP2	7.2%	7.7%	Reflux in $CHCl_3$, overnight
NP2	2.8%	2.9%	Sample analysed after catalysis

S4. Catalytic procedures

General conditions. For the reactions at 50 °C, standard 14 mL thin walled vials in a drysyn multiwell heating block (below right). The temperature regulated by an electronic contact thermometer connected to the stirrer hotplate, which was allowed to reach temperature before the vials were inserted. A drop of silicone oil in the wells was used to ensure efficient heat transfer between the block and the vials.

For the reactions at 100 °C, thick-walled vials designed for reactions at pressure were used. A blast shield was used for these experiments.

Due to the selectivity of the reaction, no side products were observed. The yield was determined through integration of the ^{1}H NMR spectra of the reaction mixture. All catalytic experiments were performed at least three times and an average taken. The accuracy of this method was assessed for the initial measurements through the use of an internal standard, 1,3,5-trimethoxybenzene (^{1}H NMR spectroscopy chemical shifts of 3.75 and 6.08 ppm). To further probe the error in the integration procedure, 1 mmol of pure benzo[*h*]quinoline was added to 1 mmol of pure 10-methoxybenzo[*h*]quinoline and dissolved in 20 mL $CDCl_3$ and the solution stirred for 10 minutes to ensure mixing of the clear solution. A sample (0.4 mL) was taken for analysis by ^{1}H NMR spectroscopy and the resonances for the H-2 (9.30 ppm, 1H) and H-10 (9.01 ppm, 1H) protons of benzo[*h*]quinoline were integrated and compared to the integral of the methoxy protons at 4.19 ppm (3H). This revealed an error of only 1-2%, providing confidence in the method.[S15]

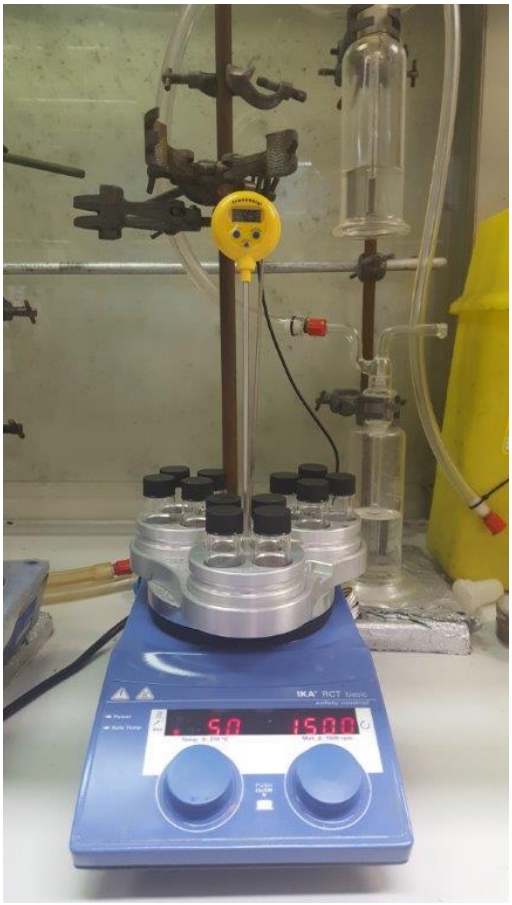

Figure S4-1. Multiwell heating block and stirrer hotplate apparatus with a thermometer.

Synthesis of 10-alkoxybenzo[*h*]quinoline (Reaction A)

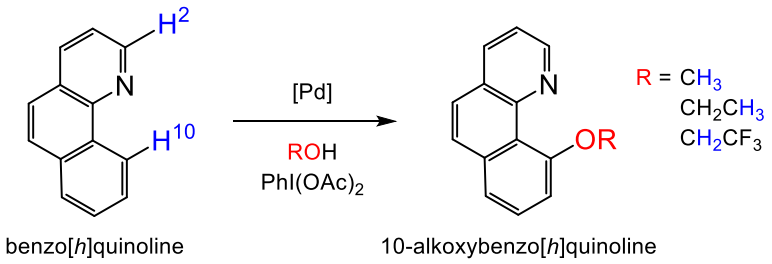

Figure S4-2. Benchmark C-H oxidative functionalization of benzo[h]quinoline.

In a typical experiment (R = Me, Et, CH_2CF_3), benzo[*h*]quinoline (50.0 mg, 0.28 mmol), (diacetoxyiodo)benzene (180.4 mg, 0.56 mmol) and the selected catalyst (1-3 mol%) were combined in the alcohol (2.5 mL) and stirred using a magnetic stir bar at 50 or 100 °C for a set time (2, 4, 6 or 24 hours). All solvent was then removed (rotary evaporation) followed by dissolution of the residue in $CDCl_3$. Integration of the diagnostic resonances in the ^{1}H NMR spectra for the H-2 (9.30 ppm) and H-10 protons (9.01 ppm) of benzo[*h*]quinoline with those of the alkoxy group in the product, which appeared at 4.19 (methoxy, CH_3), 1.63 and 4.45 (ethoxy, CH_2CH_3), 4.74 (trifluoroethoxy, CH_2CF_3) ppm.

When using the immobilized material, benzo[*h*]quinoline (20 mg, 0.13 mmol), (diacetoxyiodo)benzene (72 mg, 0.26 mmol) and **3**@SiO_2@Fe_3O_4 (**NP1**) or **4**@SiO_2@Fe_3O_4 (**NP1**) (3 mol%, calculated from ICP-OES data) were heated in methanol (2.5 mL) at 50 or 100 °C for the designated time (2 or 22 h). The solvent was removed under reduced pressure, and the resultant mixture was analyzed by ^{1}H NMR spectroscopy as before.

Reaction B: Synthesis of 8-(methoxymethyl)quinoline (Reaction B)

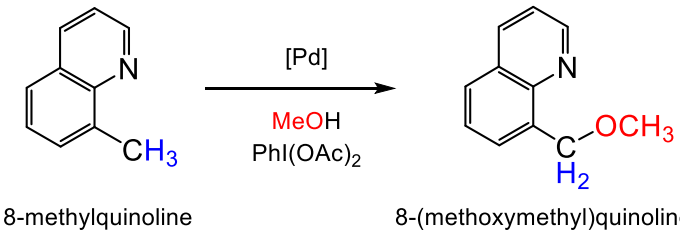

Figure S4-3. Benchmark C-H oxidative functionalization of 8-methylquinoline.

The same general procedure was used as for benzo[*h*]quinoline. Integration of the diagnostic resonances in the ^{1}H NMR spectra for the CH_3 (2.82 ppm) of 8-methylquinoline with those of the methylene group (5.19 ppm) and methoxy group (3.57 ppm) in the product.[S15]

Table S4-1. Catalytic results for the reaction of benzo[*h*]quinoline with methanol in the presence of (diacetoxyiodo)benzene. **PdDTC** = $[Pd(S_2CNEt_2)(PPh_3)_2]PF_6$.

Reaction	Catalyst	Pd (mol%)	Temperature (°C)	Time (h)	Yield (%)	SD
A	**3**	1	100	2	85	(± 0.6)
A	**4**	1	100	2	85	(± 0.7)
A	**PdDTC**	1	100	2	87	(± 1.0)

The yields in the table were obtained from ^{1}H NMR analysis and are the average of three separate experiments.

Table S4-2. Catalytic results for benzo[*h*]quinoline with ethanol and trifluoroethanol employing **3**, **4** and $[Pd(S_2CNEt_2)(PPh_3)_2]PF_6$ (**PdDTC**) as catalysts (3 mol%). Oxidant = $PhI(OAc)_2$, T = 50 °C.

Reaction	R	Catalyst	Time (h)	Yield (%)	SD
A	Et	**PdDTC**	2	89	(± 2.0)
A	Et	**3**	24	99	(± 0.4)
A	Et	**4**	24	42	(± 3.4)
A	CH_2CF_3	**PdDTC**	4	92	(±1.0)
A	CH_2CF_3	**3**	6	98	(±0.2)
A	CH_2CF_3	**4**	6	90	(±1.7)

The yields in the table were obtained from ^{1}H NMR analysis and are the average of three separate experiments.

Table S4-3. Catalytic results for 8-methylquinoline with methanol employing **4** and $[Pd(S_2CNEt_2)(PPh_3)_2]PF_6$ (**PdDTC)** as catalysts (3 mol%). Oxidant = $PhI(OAc)_2$, T = 50 °C.

Reaction	R	Catalyst	Time (h)	Yield (%)	SD
B	Me	**PdDTC**	2	66	(± 0.2)
B	Me	**4**	6	60	(± 3.8)

The yields in the table were obtained from ^1H NMR analysis and are the average of three separate experiments.

Table S4-4. Catalytic results for the reaction of benzo[*h*]quinoline with methanol in the presence of (diacetoxyiodo)benzene and various catalysts using a Pd loading of 3 mol%.

	T (°C)	Time (h)	Run 1	Run 2	Run 3	Run 4
Compound **3**	50	2	87%	-	-	-
Compound **4**	50	2	88%	-	-	-
3@SiO_2@Fe_3O_4 (**NP1**)	50	2	32%	13%	5%	-
4@SiO_2@Fe_3O_4 (**NP2**)	50	2	32%	27%	10%	6%
3@SiO_2@Fe_3O_4 (**NP1**)	50	22	76%	-	-	-

For runs 2-4, the catalyst material was captured on the side of the flask by a hand-held magnet and washed before recharging with fresh substrate and reactants.

S5. References

(S1) Blackburn, J. R.; Nordberg, R.; Stevie, F.; Albridge, R. G.; Jones, M. M. Photoelectron spectroscopy of coordination compounds. Triphenylphosphine and its complexes. *Inorg. Chem.* **1970**, *9* (10), 2374-2376, DOI 10.1021/ic50092a039.

(S2) Exarchos, G.; Nyburg, S. C.; Robinson, S. D. The synthesis and characterisation of $[Pd(S_2CNEt_2)(Ph_2PCH_2CH_2PPh_2]^+$ salts of some chloro- and bromo-metallate anions — X-ray crystal structures of $[Pd(S_2CNEt_2)(Ph_2PCH_2CH_2PPh_2)^+[MCl_2]^-$ (M = Cu, Ag). *Polyhedron*, **1998**, *17* (8), 1257-1266, DOI 10.1016/S0277-5387(97)00386-0.

(S3) Lassahn, P. G.; Lozan, V.; Wu, B.; Weller, A. S.; Janiak, C. Dihalogeno(diphosphane)metal(II) Complexes (metal = Co, Ni, Pd) as Pre-Catalysts for the Vinyl/Addition Polymerization of Norbornene – Elucidation of the Activation Process with $B(C_6F_5)_3/AlEt_3$ or Ag[*closo*-1-$CB_{11}H_{12}$] and Evidence for the *in situ* formation of "naked" Pd^{2+} as a highly active species. *Dalton Trans.* **2003**, (23), 4437-4450, DOI 10.1039/B302937A.

(S4) Kubota, M.; Ohba, S.; Saito, Y. Structure of trans-diiodobis(triphenylphosphine)palladium (II)–trichloromethane (1/1). *Acta Cryst.* **1991**, *C47* (8), 1727-1729, DOI 10.1107/S0108270191001956.

(S5) Aizawa, S. I.; Majumder, A.; Maeda, D.; Kitamura, A. Mechanism of Catalytic Chalcogen Atom Replacement of Phosphine Chalcogenides and Separation of the Intermediate Phosphine. *Chem. Lett.,* **2009***, 38* (1), 18–19, DOI 10.1246/cl.2009.18.

(S6) Park, S. K.; Kim, K. D.; Kim, H. T. Preparation of Silica Nanoparticles: Determination of the Optimal Synthesis Conditions for Small and Uniform Particles. *Colloids Surf. A* **2002**, *197* (1-3), 7-17, DOI 10.1016/S0927-7757(01)00683-5.

(S7) Rossi, L. M.; Vono, L. L.; Silva, F. P.; Kiyohara, P. K.; Duarte, E. L.; Matos, J. R. A magnetically recoverable scavenger for palladium based on thiol-modified magnetite nanoparticles. *Appl. Catal. A*, **2007**, *330*, 139–144, DOI 10.1016/j.apcata.2007.07.018.

(S8) Jacinto, M. J.; Kiyohara, P. K.; Masunaga, S. H.; Jardim, R. F.; Rossi, L. M. Recoverable Rhodium Nanoparticles: Synthesis, Characterization and Catalytic Performance in Hydrogenation Reactions. *Appl. Catal. A* **2008**, *338*, (1-2), 52–57, DOI 10.1016/j.apcata.2007.12.018.

(S9) Collinson, J. M.; Wilton-Ely, J. D. E. T.; Díez-González, S. Reusable and highly active supported copper (I)–NHC catalysts for Click chemistry. *Chem. Commun.*, **2013**, *49* (97) 11358-11360, DOI 10.1039/C3CC44371J.

(S10) SHELXTL v5.1, Bruker AXS, Madison, WI, 1998.

(S11) SHELX-2013; Sheldrick, G. M. Crystal structure refinement with SHELXL. *Acta Cryst.*, **2015**, *C71* (1), 3-8.

(S12) Sheldrick, G. M. SHELXT - Integrated space-group and crystal-structure determination. *Acta Cryst.,* **2015**, *A71*, 3-8, DOI 10.1107/S2053273314026370.

(S13) Sheldrick, G. M. A Short history of SHELX. *Acta Cryst.,* **2008**, *A64*, 112-122, DOI 10.1107/S0108767307043930.

(S14) Dolomanov, O. V.; Bourhis, L. J.; Gildea, R. J.; Howard, J. A. K.; Puschmann, H. *OLEX2*: A complete structure solution, refinement and analysis program, *J. Appl. Cryst.* **2009**, *42*, 339-341, DOI 10.1107/S0021889808042726.

(S15) Jantan, K. A.; Kwok, C. Y.; Chan, K. W.; Marchiò, L.; White, A. J. P.; Deplano, P.; Serpe, A.; Wilton-Ely, J. D. E. T. From Recovered Metal Waste to High-Performance Palladium Catalysts. *Green Chem*. **2017**, *19* (24), 5846-5853, DOI 10.1039/C7GC02678A.